Spike-Timing Patterns Conform to Gamma Distribution with Regional and Cell Type-Specific Characteristics

Abbreviated title: Brain-Wide Spike-Time Patterns

Meng Li[1], Kun Xie[1], Hui Kuang[1], Jun Liu[1], Deheng Wang[1], Grace E. Fox[1], Xiaojian Li[1], Yuhui Li[1], Fang Zhao[1], He Cui[2] & Joe Z. Tsien[1,*]

[1]Brain and Behavior Discovery Institute and Department of Neurology, Augusta University, Augusta, GA 30912, USA

[2]Institute of Neuroscience, Chinese Academy of Sciences, Shanghai 200031, China

*Correspondence should be addressed to Joe Z. Tsien, Brain and Behavior Discovery Institute and Department of Neurology, Augusta University, 1120 15th street, Augusta, GA 30912. E-mail: jtsien@augusta.edu.

Number of page: 43

Number of figures: 11

Number of words for Abstract: 190

Number of words for Introduction: 546

Number of words for Discussion: 872

Conflict of Interest: The authors declare no competing financial interests.

Acknowledgements: This work is supported by an NIH grant (R01NS079774) and GRA equipment grant to J.Z.T. and the Brain Decoding Center grant Yunnan Science Commission (2014DG002) to F.Z. and J.Z.T. We thank Prof. Yang Dan at UC Berkeley for sharing the cat dataset, which was downloaded from the CRCNS website. We thank Sandra E. Jackson for proofreading the manuscript.

Abstract Spike-timing patterns are crucial for synaptic plasticity and neural computation, yet their statistical patterns in various brain regions which cross different mammalian species have not been examined in a systematic manner. Neurons *in vivo* discharge spikes with enormous variability; this irregularity is widely viewed as noise and thus often model as a Poisson-like random process. Here, we systematically examine statistical behaviors of spike-time irregularity in 13 different cortical and subcortical regions from mouse, hamster, cat and monkey brains. We show that spike-timing patterns of various projection neurons - including cortical excitatory principal cells, hippocampal pyramidal cells, inhibitory striatal medium spiny neurons, as well as dopaminergic neurons – all conform to the gamma distribution model. Moreover, gamma shapes of spike-timing patterns remain robust over different states, such as sleep vs. awake periods. Interestingly, there are significant regional variations with DA neurons, the somatosensory cortex and motor cortices showing increased regularity, whereas the V1 cortex, retrosplenial cortex, anterior cingulate cortex, striatum, amygdala and hippocampus tend to exhibit greater irregularity. Such a conserved Gamma-distribution pattern, coupled with characteristic regional variations, may influence how spike-timing patterns exert dynamic actions on neural coding and network-level plasticity.

Significance Statement: Spike-timing patterns are crucial for synaptic plasticity and neural computation, yet their statistical patterns in various brain regions which cross different mammalian species have not been examined in a systematic manner. We have examine statistical behaviors of spike-time irregularity in 13 different cortical and subcortical regions from mouse, hamster, cat and monkey brains. We show that spike-timing patterns of various projection neurons all conform to the gamma distribution model. Furthermore, there are significant regional variations of the spike-timing's regularities. In coupling with different NMDA receptor compositions across different regions, such intrinsic statistical characteristics of spiking-time distribution will likely influence not only how spike-timing patterns drive synaptic plasticity but also how cell assemblies in various circuits perform neural computation.

Introduction

Spike-timing patterns play important roles in synaptic plasticity and neural computation (Gerstner et al., 1996; Markram et al., 1997; deCharms and Zador, 2000; Song et al., 2000; Sjostrom et al., 2001; Lisman and Spruston, 2005). During cognitions and behaviors, neurons discharge their spikes *in vivo* with tremendous variability in both the "control" resting states and across trials within the same experiments in response to identical stimuli (Shadlen and Newsome, 1994; Brown et al., 2004; Faisal et al., 2008). This variability is widely assumed to reflect noises or uncontrolled internal variables derived from synaptic, cellular and network levels (Ermentrout et al., 2008; Masquelier, 2013). Intriguingly, it is known that neurons are capable of generating precisely-timed spikes in response to fluctuating currents injected at the soma (Mainen and Sejnowski, 1995; Abbott and Sejnowski, 1999; Toups et al., 2012). It has been shown that in spite of "channel noise" (Faisal et al., 2008), deterministic neuronal models can accurately predict stimulus responses (Gerstner and Naud, 2009).

The irregularity of inter-spike intervals has long been suggested to be a fundamental process of cortical communication (Shadlen and Newsome, 1998; deCharms and Zador, 2000; Mazurek and Shadlen, 2002; Ma et al., 2006; Caporale and Dan, 2008; Gilson et al., 2011), and it was often modeled as a Poisson-like random process. Intriguingly, a growing number of observations have shown that the neuronal spike pattern in many cortical areas seems to be inconsistent with the Poisson process, indicating that the Poisson process can either under- or over-estimate the variabilities of the neuronal spike patterns (Kara et al., 2000; DeWeese et al., 2003; Lindner, 2006; Heil et al., 2007; Kang et al., 2010; Berkes et al., 2011; Li et al., 2015; Moezzi et al., 2016). Despite the importance in regulating synaptic plasticity and neural coding, spike-time patterns cross a wide range of brain regions and animal species has not been examined

or compared in a systematic manner. It remains to be demonstrated whether statistical features of spike patterns in various brain regions would conform to a particular set of mathematical properties and models (e.g. log-normal distribution, gamma distribution, and/or Poisson model). Systematic characterizations of spike-time patterns in a brain-wide manner would be valuable towards the better understanding of how neural coding is achieved and modified by synaptic plasticity upon learning.

In the present study, we set out to apply a series of statistical analyses on large-scale *in vivo* datasets of neuronal spike activity collected from 13 cortical and subcortical regions from four different animal species - namely, mice, hamsters, cats and monkeys. Our analyses show that the spike patterns of various principal projection neurons - including excitatory cortical cells, CA1 pyramidal cells, inhibitory medium spiny neurons in the striatum, as well as dopaminergic neurons from the ventral tegmental area (VTA) - all follow positive-skewed, long-tailed distribution. We then conducted goodness-of-fit analyses and demonstrate that the positive-skewed spike patterns can be statistically characterized much better by the gamma distribution model rather than the log-normal distribution model. Furthermore, we found that the overall gamma distribution shapes of the positive-skewed spike patterns remain robust against the changes of firing rates across distinct cognitive states, such as sleep vs. awake periods. However, neurons in different regions or animal species exhibit distinct tendencies in the degrees of irregularities of spike dynamics.

Materials and Methods

Ethics Statement

All animal work described in the study was carried out in accordance with the guidelines laid down by the National Institutes of Health in the United States, regarding the care and use of animals for experimental procedures, and was approved by the Institutional Animal Care and Use Committee of Augusta University (Approval AUP number: BR07-11-001).

Construction of tetrode headstages and animal surgery of the datasets of mouse BLA, CA1, ACC, RSC, STR, V1, 2nd AuV, somatosensory cortex, and hamster PrL

Tetrodes and headstages were constructed using the procedures as we have previously described (Lin et al., 2006; Xie et al., 2016b; Xie et al., 2016a). To construct tetrodes, a folded piece consisting of four wires (90% platinum, 10% iridium, 13 μm, California Fine Wire Company, Grover Beach, CA, USA) was twisted together using a manual turning device and soldered with a low-intensity heat source (variable temperature heat gun 8977020, Milwaukee, Brookfield, WI, USA) for 6 s. The impedances of the tetrodes were measured with an electrode impedance tester (Model IMP-1, Bak Electronics, Umatilla, FL, USA) to detect any faulty connections, and our tetrodes were typically between 0.7 MΩ and 1 MΩ. The insulation was removed by moving the tips of the free ends of the tetrodes over an open flame for approximately 3 s. The tetrodes were then placed into appropriate polyimide tubes. The recording ends of the tetrodes were cut differentially (Vannas spring scissors −3 mm cutting edge, Fine Science Tools, Foster City, CA, USA) according to the different depths of the recording sites. This ensures that only tetrodes, but not the surrounding polyimide tubes, were inserted into the brain tissue, thereby minimizing the tissue damage.

We employed adjustable 128-channel tetrode microdrives to target the basolateral amygdala (BLA; n = 8 WT mice), hippocampal CA1 (n = 9 WT mice), anterior cingulate cortex (ACC; n = 7 WT mice), the retrosplenial cortex (RSC; n = 20 WT mice), dorsal striatum (STR; n = 7 WT mice), primary visual cortex (V1; n = 14 WT mice), 2nd auditory cortex (2nd AuV; n = 9 WT mice), somatosensory cortex (n = 11 WT mice), and hamster prelimbic region (PrL; n = 13 WT Golden Syrian hamsters) bilaterally with 64 channels per hemisphere (Lin et al., 2006). Stereotaxic coordinates were as follows: for BLA, 1.7 mm posterior to bregma, 3.5 mm lateral, −4.0 mm ventral to the brain surface; for ACC, +0.5 mm AP, 0.5 mm ML, −1.75 mm DV; or CA1, 2.0 mm lateral to the bregma and 2.3 posteriors to the bregma; for RSC, −2.5 mm AP, 0.5 mm ML, −0.8 mm DV; for STR, +0.62 mm AP, 1.35 mm ML, −2.0 mm DV; for V1, -3.08 mm AP, 2.5 mm ML, −0.5 mm DV; for 2nd AuV, -1.94 mm AP, 4.75 mm ML; for somatosensory cortex, -1.1 mm AP, 1.5 mm ML; and for recording in the prelimbic cortex (PrL) of the Golden Syrian hamster, the stereotaxic coordinate was +3.50 mm AP, ± 0.7 mm ML, −4.0 mm DV (Paxinos and Franklin, 2004).

Male wild-type mice (6–8 months old) or adult male hamsters (3–4 months old) were moved from home cages housed in the LAS facility to the holding area next to the chronic recording rooms in the laboratory and stayed in a large plastic bucket (20 inches in diameter and 16 inches in height – per mouse, Walmart) with access to water and food for a week prior to surgery. During this period, the animals were also handled daily to minimize the potential stress from human interaction. On the day of the surgery, the animal was given an intraperitoneal injection of 60 mg/kg ketamine (Bedford Laboratories, Bedford, OH, USA) and 4 mg/kg Domitor (Pfizer, New York, NY, USA) prior to the surgery. The head of the animal was secured in a stereotaxic apparatus, and an ocular lubricant was used to cover the eyes. The hair above the surgery sites was

removed, and Betadine solution was applied to the surface of the scalp. An incision was then made along the midline of the skull. Hydrogen peroxide (3% solution, Fisher Scientific) was placed onto the surface of the skull so that bregma could be visualized. The correct positions for implantation were then measured and marked. For fixing the microdrive headstage, four holes for screws (B002SG89S4, Amazon, Seattle, WA, USA) were drilled on the opposing side of the skull and, subsequently, the screws were placed in these holes with reference wires being secured to two of the head screws. Craniotomies for the tetrode arrays were then drilled, and the dura mater was carefully removed. After the electrodes were inserted and tetrodes were secured to the fiberglass base, the reference wires from the connector-pin arrays were soldered such that there would be a continuous circuit between the ground wires from the head screws and those from the connector-pin arrays. Finally, the connector-pin arrays were coated with epoxy. Aluminum foil was used to surround the entire headstage to aid in protection and to reduce noise during recordings. The animals were then awoken with an injection of 2.5 mg/kg Antisedan. The animals were allowed to recover post-surgery for at least 3–5 days before recording began. Then, the electrode bundles targeting the BLA, STR and hippocampal CA1 region were slowly advanced over several days in small daily increments. For the cortical sites, tetrodes were advanced usually only once or twice in a small increment. At the end of the experiments, the mice were anesthetized and a small amount of current was applied to the recording electrodes in order to mark the positions of the stereotrode bundles. The actual electrode positions were confirmed by histological Nissl staining using 1% cresyl echt violet. In some experiments, for facilitating the identification of electrode array position, the electrode tips were dipped in fluorescent Neuro-DiI (Neuro-DiI, #60016, Red oily solid color, from Biotium, Inc.) which then can reveal the electrode track.

Experimental Design

We recorded mouse STR, V1, 2nd AuV, somatosensory cortex, and hamster PrL when animals were in the quiet awake state. The datasets of mouse ACC, RSC, CA1 and BLA were recorded under two distinct state: the quiet awake state and sleep state.

In vivo recording of the datasets of mouse BLA, CA1, ACC, RSC, STR, V1, 2nd AuV, somatosensory cortex, and hamster PrL

After surgery, the animals were handled for another 5–10 days while electrodes were advanced to the recording sites for obtaining the maximum neural units.

For the datasets of mouse STR, 2nd AuV, somatosensory cortex, and hamster PrL, recordings were carried out while the animals were in their home cages. Quiet-awake episodes were manually assigned when the mice were awake and immobile. Neuronal spike data during the awake state was recorded for at least 15 minutes for each animal.

For the datasets of mouse ACC, RSC, CA1 and BLA, we recorded the neuronal spike activity in both the quiet-awake state and the sleep state. Recordings were first carried out while the animals were in their home cages. To identify the sleep episodes, local field potentials were first band-pass filtered in theta band (4–12 Hz) and delta band (1–4 Hz); then the ratio of the power in theta band to that of delta band was calculated. Two criteria were applied to extract from the sleep state: (1) Duration of an epoch was longer than 5 s, and (2) the ratio of the power during an epoch was greater than mean 5SD. For each mouse, the awake and sleep states were recorded for at least 15 minutes.

For the dataset of mouse V1, we set up an experimental configuration modified from the design of a previous study (Niell and Stryker, 2010). Briefly, a tread mill (5 inches in diameter) was levitated by a stream of pressured air, the tangential force of a mouse running on the tread mill was calculated to be comparable to the force needed for free running. There was a lick port in front of the mouse's mouth, dropping sugar water every one minute. A camera with a telescope was set at the right side of the mouse eye (8cm distance) for monitoring eye movement. The mouse was implanted electrode arrays in primary visual cortex of the left hemisphere for chronic recording a week before head-fixed visual stimulation experiment. For habituation, the mouse was fixed on the top of a tread mill two hours every day, by mounting the headstage on a metal holder. An optical mouse was placed underneath the tread mill to measure the animal's movements. During the recording, the mouse was to either sit still or run on the tread mill. We found that the eye movement and animal's movement state were highly synchronized, the eye ball was almost fixed when the mouse was in still state.

Visual stimuli were generated in MATLAB and displayed on a Dell 24-inch monitor placed 27 cm in front of the right eye. Before any recordings, we calibrated the location of the monitor. Specifically, black and white dots with 1 degree to 4 degrees were randomly presented on the monitor with a 10 ms duration. The visual response of the primary visual cortex were amplified, acquired and streamed to the computer by the Plexon electrophysiology recording system. The time stamp of the visual stimulation were also sent to the Plexon simultaneously. The receptive field mapping software was written in MATLAB, which could tag the receptive field of the recorded neurons on the monitor, based on the e-phys data. Then we adjusted the location of the monitor to make sure the neuron group receptive field to be located in the center of the monitor.

Two different visual stimuli were employed in the formal recording: 1. Full-length drifting bars [combinations of eight orientations (π/8, π/4, π3/8, π/2, π5/8, π3/4, π7/8 and π), four spatial frequencies (0.25, 0.5, 1 and 2 Hz), four temporal frequencies (0.25, 0.5, 1 and 2 Hz) and two directions (drifting either left or right)]; 2. Two-dimensional stimuli [we recorded 624 gray-scale images of 78 objects (42 toy animals and 36 toy cars), each object was recorded from eight different viewing directions in a 45º interval]. For each recording section, one of these three visual stimuli was delivered. At least 30 minutes of neuronal spike data was recorded during each recording section. Basically the mice stayed on the tread mill without struggling for more than 2 hours, then we free then to the home cages.

Cell-type classification in mouse BLA, ACC, RSC, STR, CA1 and hamster PrL

For the datasets recorded from mouse BLA, ACC, RSC, STR, CA1 and hamster PrL, well-isolated units were classified as either putative excitatory principal cells or inhibitory interneurons based on three characteristic features of their spike activities - namely, trough-to-peak width, half-width after trough, and the mean firing rates. The k-means method was employed to achieve automated cell-type clustering. In general, putative principal cells fire at lower rates and have broader waveforms, whereas interneurons have higher rates and relatively narrower waveforms.

Animal surgery and *in vivo* recording of mouse VTA dataset

The details have been previously described (Wang and Tsien, 2011). A 32-channel (a bundle of eight tetrodes) electrode array was constructed. One week before surgery, mice (3–6 months old) were removed from the standard cages and housed in customized home cages (40×20×25 cm). On the day of surgery, the mice were anesthetized with Ketamine/Xylazine (80/12 mg/kg, i.p.); the electrode array was then

implanted toward the VTA in the right hemisphere (3.4 mm posterior to bregma, 0.5 mm lateral and 3.8–4.0 mm ventral to the brain surface) and secured with dental cement.

Two or three days after surgery, the electrodes were screened daily for neural activity. If no dopamine neurons were detected, the electrode array was advanced 40~100 μm daily, until we could record from a putative dopamine neuron. In brief, spikes (filtered at 250–8000 Hz; digitized at 40 kHz) were recorded during the entire experimental process using the Plexon multichannel acquisition processor system (Plexon Inc.). Mice behaviors were simultaneously recorded using the Plexon CinePlex tracking system. Recorded spikes were isolated using Plexon OfflineSorter software. Dopamine neurons were distinguished from other neurons in the region by the characteristics of their extracellularly recorded impulses - including long, multiphasic waveforms and low basal firing rates.

Monkey area 5d dataset

The dataset was previously described (Li and Cui, 2013). Data were recorded from two male rhesus monkeys (Macaca mulatta, 7-10 kg). The animals were trained to perform visually guided single- and double-arm reaching tasks. All procedures were in accordance with NIH guidelines and were approved by the Institutional Animal Care and Use Committee of Augusta University. Recorded spikes were re-sorted using Plexon OfflineSorter software; multiple spike-sorting parameters (e.g., principle component analysis, energy analysis) were used for the best isolation of single-unit spike trains. Because of the absence of the spike waveform information, we were not able to separate different neuron types (excitatory vs. inhibitory cells, etc.). However, we observed that the conclusion that neuronal spike activities can be best described by the gamma distribution model still hold true in the monkey area 5d region.

Cat V1 Datasets

The cat V1 datasets (1-D and 2-D) were downloaded from the Collaborative Research in Computational Neuroscience (CRCNS) website (data from Yang Dan Lab at UC-Berkeley, download link: http://crcns.org/data-sets/vc/pvc-2). Experimental procedures have been previously described (Touryan et al., 2002; Felsen et al., 2005; Touryan et al., 2005). The data were obtained with extracellular recordings from the primary visual cortex of anesthetized adult cats. Because of the absence of the spike waveform information, we were not able to separate different neuron types. However, we observed in conclusion that neuronal spike activities can be best described by the gamma distribution model and still hold true in the monkey area 5d region.

Data processing and spike-sorting

Neuronal activities from mouse experiments were recorded by the MAP system (multi-channel acquisition processor system, Plexon Inc., Dallas, TX) in the manner as previously described (Kuang et al., 2010). Extracellular action potentials and local field potentials data were recorded simultaneously and digitized at 40 kHz and 1 kHz, respectively. The artifact waveforms were removed and the spike waveform minima were aligned using the Offline Sorter 2.0 software (Plexon Inc., Dallas, TX), which resulted in more tightly clustered waveforms in principal component space. Spike sortings were done with the MClust 3.3 program with an auto-clustering method (KlustaKwik 1.5). Only units with clear boundaries and less than 0.5% of spike intervals within a 1 ms refractory period were selected. The stability of the *in vivo* recordings was judged by waveforms at the beginning, during and after the experiments. Well-separated neurons were assessed by “Isolation Distance” (Schmitzer-Torbert et al.,

2005). Neurons whose "Isolation Distance" >15 were selected for the present analysis as described previously (Lin et al., 2006; Xie et al., 2016b; Xie et al., 2016a).

Statistical Analysis

As shown in Figure 5, *t*-test was used to assess whether k (or θ) were linear correlated between the quiet awake state and the sleep state. In Figure 11, one-way ANOVA analysis and Tukey post hoc tests were conducted for the comparisons of multiple means of k across different brain regions. three asterisks denoted the p-value is less than 0.001. Data were represented as mean ± SEM.

Statistical properties of neural spike patterns

A two-step analysis was employed to examine the statistical properties of neural spike patterns.

Step 1: Positive-skewed vs. negative-skewed distributions. The distribution of ISI was characterized by two well-defined statistics - namely, nonparametric-skew (S) and skewness (γ), defined as follows:

$$S = \frac{\mu - \upsilon}{\sigma} \tag{1}$$

$$\gamma = \mathrm{E}\left[\left(\frac{I-\mu}{\sigma}\right)^3\right] = \frac{\mathrm{E}\left[(I-\mu)^3\right]}{\left(\mathrm{E}\left[(I-\mu)^2\right]\right)^{3/2}} \tag{2}$$

where μ is the mean, υ is the median, σ is the standard deviation, E is the expectation operator, and I denotes the ISIs of a neuronal spike train.

In probability theory and statistics, nonparametric-skew (S) and skewness [$\gamma \in (-\infty, +\infty)$] are measurements of the skewness (or long-tailedness) of a random variable's distribution – that is, the distribution's tendency to lean to one side or the other of the mean (Figure 1B). A positive-skewed distribution (red curve in Figure 1B) has $S > 0$ and $\gamma > 0$, a negative-skewed distribution (blue curve in Figure 1B) has $S < 0$ and $\gamma < 0$, while a symmetric distribution (gray dotted curves in Figure 1B) has $S = 0$ and $\gamma = 0$.

Step 2: Gamma distribution vs. log-normal distribution. Let $I_1, I_2, \cdots I_n$ denote the ISIs of a neuron's spike train, the probability density function for a gamma distribution of I is defined by a shape parameter $k > 0$ and a scale parameter $\theta > 0$:

$$f_{GA}(i; k, \theta) = \frac{1}{\Gamma(k)\theta^k} i^{k-1} e^{-\frac{i}{\theta}} \tag{3}$$

where $\Gamma(k)$ is the gamma function.

The probability density function of a log-normal distribution of I is defined by a location parameter $\mu \in$ □ and a scale parameter $\sigma > 0$:

$$f_{LN}(i; \mu, \sigma) = \frac{1}{\sqrt{2\pi} i \sigma} e^{-\frac{(\ln i - \mu)^2}{2\sigma^2}} \tag{4}$$

In the present analyses, both gamma distribution and log-normal distribution were estimated using the maximum likelihood estimates (MLE) method, which selected values of parameters that produced corresponding distributions for the histograms of ISI with minimal errors.

Goodness-of-fit analyses were then conducted to quantitatively discriminate between the gamma distribution and log-normal distribution models. For convenience, we termed a gamma distribution and a log-normal distribution as $GA(k,\theta)$ and $LN(\mu,\sigma)$, respectively. Thus, the likelihood functions of data that follow $GA(k,\theta)$ and $LN(\mu,\sigma)$ can be denoted as:

$$L_{GA}(k,\theta)=\prod_{j=1}^{n} f_G\left(i;k,\theta\right) \tag{5}$$

$$L_{LN}(\mu,\sigma)=\prod_{j=1}^{n} f_{LN}\left(i;\mu,\sigma\right) \tag{6}$$

Therefore, the RML between a gamma distribution and a log-normal distribution is defined as:

$$RML=\frac{L_{GA}(\hat{k},\hat{\theta})}{L_{LN}(\hat{\mu},\hat{\sigma})} \tag{7}$$

where $(\hat{k},\hat{\theta})$ and $(\hat{\mu},\hat{\sigma})$ are the MLEs of (k,θ) and (μ,σ) for I. The natural logarithm of RML can be written as:

$$D=n\left[\hat{k}\ln\left(\frac{\tilde{I}}{\hat{\theta}}\right)+\frac{1}{2\hat{\sigma}^2 n}\sum_{j=1}^{n}\left(\ln\left(\frac{I_j}{\hat{\mu}}\right)\right)^2+\frac{1}{2}\ln\left(2\pi\right)-\ln\left(\frac{\Gamma\left(\hat{k}\right)}{\hat{\sigma}}\right)-\frac{\bar{I}}{\hat{\theta}}\right] \tag{8}$$

where $\bar{I}=\frac{1}{n}\sum_{j=1}^{n} I_j$ and $\tilde{I}=\left(\prod_{j=1}^{n} I_j\right)^{\frac{1}{n}}$ are the arithmetic and geometric means of I, respectively.

The natural logarithm of RML, D, measured the goodness-of-fit between the gamma distribution model and the log-normal distribution model of ISI. That is, the gamma distribution model precedes the log-normal distribution model if $D > 0$; otherwise, choose the log-normal distribution as the preferred model of ISI. The larger the absolute value of D, the more accurate-fitting the result of the chosen model over the other model.

Results

Statistical properties of neural spike patterns

Neural spike activities are highly variable even in the quiet-awake resting state (upper subpanel of Figure 1A), and the distributions of the single unit's spike patterns showed that they are skewed with heavy tails (lower subpanel of Figure 1A). Thus, we set out to conduct a two-step analysis to explore the statistical properties of neural spike patterns.

Step 1: Does the neural spike pattern follow a positive-skewed or negative-skewed distribution (Figure 1B)? We characterized the distribution of inter-spike intervals (ISIs) for neural spike patterns by using two well-defined statistics - namely, nonparametric-skew (S) and skewness (γ) (see Materials and Methods). In probability theory and statistics, these two parameters are measurements of the skewness (or long-tailedness) of a random variable's distribution – that is, the distribution's tendency to lean to one side or the other of the mean (Figure 1B). A positive-skewed distribution (red curve in Figure 1B) has $S>0$ and $\gamma>0$, a negative-skewed distribution (blue curve in Figure 1B) has $S<0$ and $\gamma<0$, while a symmetric distribution (gray dotted curves in Figure 1B) has $S=0$ and $\gamma=0$.

Step 2: We then considered the problem of selecting the best-fitting statistical distribution model to characterize this positive-skewed distribution. As two widely-used distributions for modeling and analyzing skewed non-negative datasets - namely, the gamma distribution model and the log-normal distribution model – these models were considered as alternatives for comparison (see Materials and Methods). The gamma distribution and log-normal distribution were previously applied for modeling firing

patterns of neuron population (Mizuseki and Buzsaki, 2013) and spike patterns of single neurons (Maimon and Assad, 2009; Pipa et al., 2013).

In Figure 1C, the ISI distribution shown in Figure 1A was analyzed here as an illustrative example. It is evident that the gamma distribution model provided more accurate fitting results than the log-normal distribution model. We then conducted goodness-of-fit analyses to quantitatively discriminate between the gamma distribution and log-normal distribution models. The ratio of maximized likelihoods (RML), which is a statistical test used for comparing the goodness-of-fit of two models (Cox, 1961, 1962, 2013), was employed for comparing the gamma distribution model and the log-normal distribution model.

The natural logarithm of RML, D, measured the goodness-of-fit between the gamma distribution model and the log-normal distribution model of ISI (see Materials and Methods). That is, the gamma distribution model precedes the log-normal distribution model if $D > 0$; otherwise, choose the log-normal distribution as the preferred model of ISI. The larger the absolute value of D, the more accurate fitting the result of the chosen model over the other model.

In the following sections, we conducted this two-step analyses on *in vivo* datasets of neuronal spike activity recorded from a wide range of cortical and subcortical areas under one or multiple brain states or experimental conditions in mice, hamsters, cats and monkeys.

Neuronal spike patterns of principal cells followed gamma distribution across different brain regions of mice under the quiet-awake state

First, we used 128-channel tetrode arrays to record large numbers of neurons from four cortical and subcortical regions - namely, anterior cingulate cortex (ACC),

retrosplenial cortex (RSC), hippocampal CA1 and the basolateral amygdala (BLA), respectively - in freely behaving mice. The qualities of recorded neurons were quantitatively measured by "Isolation Distance" (Schmitzer-Torbert et al., 2005), and only neurons whose "Isolation Distance" >15 were selected for the present analysis. To facilitate direct comparison, we focused on putative principal cells after being separated from fast-spiking putative interneurons (see Materials and Methods). In addition, to minimize the potential state-dependent influence on neuronal variability, we used the spike datasets collected from the quiet-awake state as animals rested in their home-cage environments.

We calculated nonparametric-skew (S) and skewness (γ) on four putative principal cell datasets recorded from four brain regions - namely, ACC (neuron number n = 197), RSC (n = 321), hippocampal CA1 (n = 511) and BLA (n = 451). Our results showed that all the principal cells in these four brain regions exhibited similar positive-skewed distributions (Figures 2A-D). Skewness (γ) had a range of 1-10 (ACC = 3.82 ± 0.11, RSC = 2.98 ± 0.07, CA1 = 3.92 ± 0.08 and BLA = 3.55 ± 0.09, data were shown as mean ± SEM). Nonparametric-skew (S) were all in a range of 0.2-0.5 (ACC = 0.346 ± 0.003, RSC = 0.335 ± 0.001, CA1 = 0.335 ± 0.002 and BLA = 0.358 ± 0.003, data were shown as mean ± SEM). These results clearly demonstrated that the neuronal spike patterns in these four brain regions of mice followed positive-skewed, long-tailed distributions.

We then fitted the spike patterns of each principal cell in four brain regions when animals were in the quiet-awake state, the parameters of gamma and log-normal distributions were estimated by the MLE method. To avoid the under-sampled error due to few data points, units with <250 ISIs were excluded in the present analysis. The left

subpanels of Figures 3A-D showed fitted gamma and log-normal distributions of example principal cells for these four regions. We calculated the natural logarithm of RML, D, for the fitted gamma and log-normal distributions for each of the principal cells in the four brain regions. As shown in the right subpanels of Figures 3A-D, $D > 0$ was observed for all putative principal cells in the four regions, indicating that the gamma distribution model achieved superior performance on fitting neuronal spike ISIs over the log-normal distribution model. Furthermore, the firing rates and D were highly linearly correlated in all four regions, and D increased with higher firing rates (the correlation coefficients between firing rates and D were: 0.80 of ACC, 0.89 of RSC, 0.83 of CA1 and 0.70 of BLA).

Spike patterns of principal cells followed gamma distribution across different cortical and subcortical regions of mice during the animals' sleep

Second, since firing patterns could vary significantly in different brain states, we asked whether the gamma distribution model provided a modest description of neuronal spike activities over different brain activity states. As such, we compared the gamma distribution and the log-normal distribution in modeling neuronal activities of principal cells recorded from the same four mice's brain regions during the animals' sleep. As shown in Figure 4, the gamma distribution model outperformed the log-normal distribution model for fitting the putative principal cells during the animals' sleep ($D > 0$ for all four brain regions). Again, the firing rates of principal cells in these four regions were also linearly correlated with D under the sleep state (the correlation coefficients between firing rates and D were: 0.93 of ACC, 0.71 of RSC, 0.86 of CA1 and 0.62 of BLA).

All these analyses supported the notion that the positive-skewed distribution of neuronal spike patterns can be statistically described by a gamma distribution model in the different cortical and subcortical regions of mice under distinct brain states.

Preserved shape parameter *k* across brain states

Since the positive-skewed distribution is an intrinsic characteristic of a neuronal spike pattern, we further examined whether there existed any invariant features across distinct brain states. Two parameters of the gamma distribution model, shape parameter k and scale parameter θ, were measured under two distinct brain states (the quiet-awake vs. sleep). In the gamma distribution model, the shape parameter k describes the overall envelope of a neuron's ISI distribution, and the scale parameter θ is related to the mean firing rate within the uncertain state (the reciprocal of the scale parameter, $r = 1/\theta$, is known as the rate parameter). The shape parameter k provides useful measurements for spike dynamics under different cognitive states, with a higher k indicating more regular spiking discharge patterns and a lower k indicating more irregular spike trains.

Analyses were performed on four additional datasets consisting of putative principal cells recorded from four brain regions under both the quiet-awake state and the animals' sleep (34 cells from ACC, 102 cells from RSC, 43 cells from CA1 and 182 cells from BLA). The analyses showed that the two parameters of the gamma distribution model were correlated between awake and sleep states in all four regions (Figure 5, correlation coefficient R between k_{awake} and k_{sleep}: ACC, R = 0.89; RSC, R = 0.91; CA1, R = 0.94; BLA, R = 0.77. Correlation coefficient R between θ_{awake} and θ_{sleep}: ACC, R = 0.81; RSC, R = 0.71; CA1, R = 0.79; BLA, R = 0.48. Ps <0.0001, *t*-test).

We further fitted these two parameters with linear functions for visually displaying the changing trends across different states by the slope of fitted linear dependencies (shown as the red lines and red numbers in Figure 5). We observed that the transformations of the scale parameter θ between awake and sleep states were varied among these brain regions. The firing rates of the principal cells in ACC remained unchanged between the two states (in the right subpanel of Figure 5A, the slopes of fitted linear dependencies was 1.003). The principal cells in RSC exhibited increased firing rates in the sleep state (in the right subpanel of Figure 5B, the slopes of fitted linear dependencies was 0.835). However, as shown in the right subpanels of Figures 5C and D, the slopes of fitted linear dependences of CA1 and BLA regions were 1.138 and 1.512, respectively, indicating that the mean firing rates of the principal cells in these two regions decreased in sleep states compared to awake states.

Contrary to the diverse transformations of the scale parameter θ, our analyses showed that the shape parameter k of the principal cells in all these four brain regions were not only highly correlated but also remained tightly preserved between the two states (the left subpanels of Figures 5A-D, as denoted by the slopes of fitted linear dependences of k: ACC, 1.056; RSC, 1.045; CA1, 1.010 and BLA, 1.027). Given the fact that the shape parameter k is a parameter for characterizing the overall shape of ISI distribution, our results provided strong evidence for the notion that the overall shapes of positive-skewed distributions of neuronal firing patterns were preserved across distinct brain states (sleep vs. awake) that is independent of the change in firing rates under different cognitive states.

Neuronal spike-activity patterns of striatal medium spiny projection neurons followed gamma distribution

The above analyses have shown that the neuronal spike patterns of the principal excitatory cells across different cortical and subcortical regions followed gamma distribution. Next, we investigated whether the gamma-like spike patterns reflect a general property that would remain true even for GABAergic projection neurons. Thus, we employed 128-channel recording techniques and monitored activity patterns from the dorsal striatum of freely behaving mice when the animals were in the quiet-awake state. We conducted the same statistical analysis on a dataset of 294 medium spiny projection neurons (see Materials and Methods). Being the principal projection neurons of the striatum, medium spiny projection neuron is a special type of GABAergic inhibitory cells distinct from many other types of local interneurons (Preston et al., 1980; Surmeier et al., 2007).

Figure 6A showed the fitted gamma and log-normal distributions of a sample medium spiny neuron, it was evident that the gamma distribution model produced a better result for the peak of the ISI distribution. As shown in Figure 6B, skewness $\gamma = 3.77 \pm 0.10$ and nonparametric-skew $S = 0.357 \pm 0.003$ (data were shown as mean ± SEM). These results show that the neuronal spike patterns of medium spiny projection neurons also exhibited positive-skewed, long-tailed distributions. Furthermore, the gamma distribution model achieved superior performance fitting neuronal spike patterns of medium spiny projection neurons over that of the log-normal distribution model ($D > 0$ for all medium spiny projection neurons, as shown in Figure 6C).

Neuronal spike-activity patterns of VTA dopaminergic neurons followed gamma distribution

To further evaluate the general utility of the gamma distribution model, we then analyzed neuromodulatory projection neurons, such as dopaminergic (DA) neurons

recorded from the VTA region in the mouse brain. We used the DA neuron datasets that we collected previously from freely behaving mice during the awake period (Wang and Tsien, 2011; Li et al., 2015). DA neurons are well-known to subserve a wide range of biological functions, such as motivation and reward (Wise, 2004; Everitt and Robbins, 2005; Bromberg-Martin et al., 2010; Schultz, 2013), addiction (Grace, 2000; Berridge et al., 2009), fear memory and behaviors (Pezze and Feldon, 2004; Fadok et al., 2009; Wang and Tsien, 2011; Abraham et al., 2014). They project over long distances to various cortical and subcortical sites (Swanson, 1982; Lammel et al., 2011; Beier et al., 2015).

As illustrated in Figure 7A, we found that the ISI distribution of a sample VTA DA neuron can be better characterized by the gamma distribution. Skewness ($\gamma = 2.55 \pm 0.29$, mean ± SEM) and nonparametric-skew ($S = 0.266 \pm 0.018$, mean ± SEM) demonstrated that the neuronal spike patterns of VTA DA neurons followed positive-skewed distributions with heavy tails (Figure 7B). Again, the gamma distribution model outperformed the log-normal distribution model for fitting the neuronal spike patterns of VTA DA neurons ($D > 0$ for all VTA DA neurons, as shown in Figure 7C). And the firing rates were linearly correlated with D (the correlation coefficients between firing rates and D was 0.60).

Taken together, our above analyses have shown that spike-timing patterns in these long-projection principal neurons all followed gamma distribution, regardless of cortical/subcortical regions, brain states, and distinct cell types (cortical excitatory cells, CA1 pyramidal cells, medium spiny neurons, or DA neurons). In the following section, we conducted comparative analyses on neuronal spike datasets recorded from

additional mammalian species to examine if the gamma-like neuronal spike patterns were universal properties of neuronal spike activities.

Neuronal spike-activity patterns of principal cells in the hamster prelimbic region followed gamma distribution

We asked whether the excitatory units in the prelimbic region (PrL) of Golden Syrian hamsters would follow the gamma-like spike patterns. As described in our previous study (Xie et al., 2016b), we implanted 64-channel tetrode arrays bilaterally into the PrL region and recorded neural-activity patterns when animals were in their quiet-awake states. A total of 200 putative excitatory principal cells recorded from 13 hamsters were identified as stable and well-isolated, and subsequently subjected to the analyses.

The gamma and log-normal models of a sample PrL principal cell were shown in Figure 8A. The spike patterns of these cells exhibited clearly positive-skewed, heavy-tailed distributions (Figure 8B, $\gamma = 3.78 \pm 0.12$, $S = 0.341 \pm 0.003$, mean ± SEM). The goodness-of-fit analysis showed that all PrL excitatory principal cells can be better described by using the gamma distribution models (Figure 7C, $D > 0$ for all PrL excitatory principal cells), and D was linearly correlated with the firing rates (correlation coefficient is 0.79). Together, these putative principal cells in the hamster PrL cortex also followed the gamma distribution model.

Neuronal spike-activity patterns of neurons in the posterior parietal cortex area 5d of monkeys followed gamma distribution

In addition to the analysis of neuronal spike patterns recorded in mouse and hamster brains, we further asked whether spike-time patterns in other higher species also followed the gamma distribution. We analyzed single-neuron datasets collected

from rhesus monkeys (Li and Cui, 2013). In this study, we recorded the single-neuron activity from the dorsal area 5 (area 5d) on the gyral surface adjacent to the medial bank of the intraparietal sulcus, which is closely linked to movement kinematics (Hamel-Pâquet et al., 2006) and movement preparation (Cui and Andersen, 2011). Briefly, the monkey was required to touch the fixation center at the trial beginning. Then, the first- and second- reach goals were simultaneously displayed for 400 ms with a green square and triangle (shifted by 135° counter-clockwise from the square), respectively. After a 600 ms delay, the central green dot turned off (GO signal), and the monkey was allowed to initiate the reaching sequence to touch the locations previously cued by the square and triangle in the correct order. Throughout the trial, the monkey was either required to maintain eye fixation (fixation condition) at the center or allowed to move his eyes freely (free-view condition). Single-reach trials were pseudo-randomly interleaved with the double-reach trials for control. Here, we analyzed a total of 211 neurons and observed that the spike patterns of monkey area 5d neurons also exhibited obvious positive-skewed distributions (Figures 9A and B, $\gamma = 17.81 \pm 1.37$, $S = 0.219 \pm 0.007$, mean ± SEM), and $D > 0$ for all area 5d neurons (Figure 9C, the correlation coefficient between firing rates and $D > 0$ was 0.42).

Neuronal spike-activity patterns of neurons in the primary visual cortex of cats followed gamma distribution

Finally, we used a dataset of extracellular recordings from the primary visual cortex of anesthetized adult cats that were deposited in the public domain (Dan et al., 2009). This dataset was originally performed to measure the spatiotemporal receptive fields of cortical cells (Touryan et al., 2002; Felsen et al., 2005; Touryan et al., 2005; Dan et al., 2009). One of two different visual stimuli, either 1-D white noise [473 neurons, one-dimensional white noise (random bars) aligned to the preferred orientation of each

cell] or 2-D stimuli (202 neurons, natural images, natural phase, and random phase), were delivered to the anesthetized cats. Thus, this dataset was not only ideal for verifying the gamma distribution model but also afforded an opportunity to examine if the gamma distribution model was robust under two different types of stimulus conditions.

First, we observed that the spike patterns of the neurons in the primary visual cortex of cats all followed positive-skewed distribution under 1-D white noise (Figures 10A and C, $\gamma = 2.80 \pm 0.04$, $S = 0.421 \pm 0.004$, mean ± SEM) and 2-D stimuli (Figures 10B and D, $\gamma = 2.81 \pm 0.05$, $S = 0.392 \pm 0.006$, mean ± SEM). Furthermore, the distributions of γ and S showed no significant differences under these two distinct types of stimuli ($p > 0.94$, *t*-test). Second, the goodness-of-fit analysis demonstrated that the gamma distribution outperformed the log-normal distribution for characterizing the spike patterns of the primary visual cortex neurons under both 1-D white noise and 2-D stimuli (Figures 10E and F, the correlation coefficients between firing rates and D were 0.44 for 1-D white noise and 0.41 for 2-D stimuli). These results show that spike patterns in the primary visual cortex of cats also followed the gamma distribution model, and overall gamma distribution remained robust over different stimulus types.

Regularities of neuronal spike patterns across distinct brain regions of different species

Given the critical roles of spike-timing patterns in synaptic plasticity and neural computations, we set out to ask how spike dynamics vary over different brain regions. Therefore, we systematically compared the regularities of neuronal spike patterns in a wide range of brain regions and further included additional datasets we have collected from the V1 cortex, secondary auditory cortex, and somatosensory cortex of behaving mice. The total datasets consisted of a total of 3,186 neurons obtained from 13 brain

regions of four species. Specifically, we analyzed datasets collected from nine mouse brain regions as follows: 29 DA neurons from the VTA, 85 putative excitatory principal cells from the somatosensory cortex, 615 excitatory principal cells from the RSC, 342 excitatory principal cells in the V1, 325 putative CA1 pyramidal cells, 41 excitatory principal cells recorded from the 2nd auditory cortex (2nd AuV), 195 excitatory principal cells from the ACC, 263 putative pyramidal cells in the BLA, and 221 putative medium spiny neurons in the STR. Moreover, we further analyzed 182 excitatory principal cells from the hamster PrL; 207 excitatory principal cells from the cat V1 area during 2-D stimuli and 475 units in the cat V1 during 1-D white noise, as well as 206 excitatory cells in the monkey brain area 5d.

We compared the regularities of neuronal spike patterns in these brain regions by examining the shape parameters k of their gamma distribution patterns. Based on its definition, k provides an effective way to measure neuronal spike patterns' regularities. gamma distribution with k=1 as the mathematical equivalent to the exponential distribution, and the neuronal spike pattern fits a Poisson process (the gray horizontal line in Figure 11). Neuronal spike patterns with $k<1$ indicate that the neuron discharges more frequently in short and long intervals than the exponential distribution – namely, irregular spiking. When $k>1$, the peaks of ISI distributions shift away from zero, and the neuron discharges more regular spiking than the Poisson process. Gamma distribution with $k=\infty$ is the distribution of no variance, and the corresponding neuronal spike pattern is perfectly regular.

As shown in Figure 11, we observed that the neuronal spike patterns in most brain regions exhibited more irregular spiking than the Poisson process [k : 0.921±0.008 in RSC, 0.844±0.015 in V1, 0.825±0.010 in CA1, 0.793±0.018 in Hamster PrL,

0.719±0.040 in 2nd AuV, 0.689±0.015 in ACC, 0.632±0.013 in BLA, 0.601±0.014 in STR, 0.636±0.013 in Cat V1 (2-D), and 0.530±0.007 in Cat V1 (1-D), data were shown as mean ± SEM]. While neurons in the other three brain regions discharged more regular spiking than the Poisson process (k : 1.755±0.162 by DA neurons from the mouse VTA, 1.610±0.055 in the monkey brain motor area 5d, and 1.240±0.039 in the mouse somatosensory cortex, data were shown as mean ± SEM), there were signficant statistical differences between three more regular-spiking regions in comparison to those of 10 irregular-spiking regions ($p < 0.0001$, One-way ANOVA coupled with Tukey's post-hoc test).

Discussion

Although spiking-timing patterns are crucial for synaptic plasticity and neural computation, statistical behaviors of spike dynamics across a brain-wide regions and multiple animal species were rarely examined. In the present study, we have performed a comprehensive characterization of spike patterns of principal projection neurons over a dozen different brain regions in four different animal species. We showed that neuronal spike patterns exhibited positive-skewed, long-tailed distributions. Furthermore, these positive-skewed distributions of neuronal spike patterns followed the gamma distribution model. Our analyses provided several detailed insights.

First, according to the independent spike hypothesis that the generation of each spike is independent of all the other spikes, the neuronal spike train would be completely described as a particular kind of random process called a Poisson process. If the Poisson process holds true for the neuronal spike-activity patterns, ISI distribution would be statistically described by an exponential distribution model. However, there are certain important features of neuronal firing that may render this simplistic assumption unsatisfactory or inaccurate to capture spike-time patterns. For example, burst-firing and the refractory periods after the generations of spikes can make neuronal spike patterns deviate away from a Poisson process (exponential distribution model). Indeed, our analysis repeatedly found that spike-time dynamics from the above 13 brain regions all exhibited the positive-skewed, heavy-tailed distribution that can be best characterized by the gamma distribution model.

Second, previous studies have reported that many variables of brain parameters (e.g., firing-rate distributions of neurons, the number of synaptic contacts between neurons, and the size of dendritic boutons) had a positive-skewed, long-tailed

distribution - typically found in log-normal distribution (Mizuseki and Buzsaki, 2013; Buzsaki and Mizuseki, 2014). For example, recent quantifications of cortical principal neurons have shown that the mean firing rates of individual neurons can span at least four orders of magnitude and that the firing-rate distribution of both stimulus-evoked and spontaneous activity in cortical neurons conformed to the log-normal distribution model. While we found that spike-timing patterns of single neurons followed a positive-skewed distribution, interestingly, the goodness-of-fit analysis demonstrated that the inter-spike interval of various neurons can be best described by the gamma distribution model. Strikingly, such gamma-distribution statistical patterns are highly conserved across different principal projection neurons, including cortical cells, CA1 pyramidal cells, medium spiny inhibitory neurons, and DA neurons - as well as across different animal species.

Third, despite the fact that neurons' firing rates vary between distinct states (as shown by the scale parameter θ in the right subpanels of Figures 5A-D), we found that the overall shapes of the neuronal spike patterns are preserved among different states (as shown by the scale parameter k in the left subpanels of Figures 5A-D). One hypothesis behind this phenomenon is that while the energy level within the neuronal circuit under distinct brain activity states may boost or lessen the firing rates of single neurons, the statistical characteristics of spike-timing patterns remain robust. This preserved statistical characteristic may be determined by preconfigured, skewed synaptic connections and/or intrinsic electrical/chemical attributes of a neuron. This characteristic also offers the potential of estimating a neuron's spike pattern among distinct states. For example, as shown in Figure 5, instead of recording a single neuron's spike train for a long period to get the statistical distribution of its spike pattern in the awake state, one can predict it by using the shape parameter k calculated in the

sleep state and/or a mean firing rate within a shorter period in the awake state. Whether this feature holds true for other distinct brain states will require further investigation.

Finally, according to the principle of maximum entropy, a neuronal spike pattern should follow an exponential distribution which indicates a Poisson process. That is, exponential distribution is the maximum entropy distribution among all continuous distributions supported in [0, ∞]. However, instead of showing exponential distribution, the neuronal spike-timing patterns all follow gamma distributions, suggesting a potential knowledge gap between information entropy and information coding. One interesting characteristic is that different brain regions seem to exhibit different degrees of spike irregularities. We found the principal neurons in three brain regions show significantly more regularity in spike-time patterns - namely, DA neurons in the VTA, excitatory principal cells from the somatosensory cortex of the mouse brain, and the monkey parietal area 5d. In contrast, principal neurons in the mouse and cat V1 cortex - as well as principal neurons from the mouse retrosplenial cortex, secondary auditory cortex, anterior cingulate cortex, striatum, amygdala and hippocampal CA1 pyramidal cells - tend to exhibit greater irregularity. Given that internal brain states (such as attention) are known to reduce neuronal variability (Mitchell et al., 2007; Cohen and Maunsell, 2009; Mitchell et al., 2009), it will be highly interesting to investigate whether such regional variations reflect the underlying molecular and cellular differences (e.g., different cholinergic inputs or receptor expression profiles). In coupling with different NMDA receptor compositions across different regions (Monyer et al., 1992; Sheng et al., 1994; Tang et al., 1999; Cui et al., 2013; Jacobs et al., 2014), such intrinsic statistical characteristics of spiking-time distribution will likely influence not only how spike-timing patterns drive synaptic plasticity (Song et al., 2000; Lisman and Spruston, 2005) but also

how cell assemblies in various circuits perform neural computation (Buzsaki, 2010; Gupta et al., 2010; Xie et al., 2016b).

Author Contributions: J.Z.T. and M.L. conceived and designed the project. J.Z.T. designed the experiments with M.L., K.X., H.K., G.E.F. and J.L. The research was performed as follows: K.X. recorded from the ACC and PrL datasets; G.E.F. from the RSC; Jun Liu from the BLA; D.W. from the striatum, H.K. for the CA1, M.L., F.Z. and H.K. for data analyses together with J.Z.T. J.Z.T. and M.L. wrote the paper with input from all others.

References

Abbott L, Sejnowski TJ (1999) Neural codes and distributed representations: foundations of neural computation: Mit Press.

Abraham AD, Neve KA, Lattal KM (2014) Dopamine and extinction: a convergence of theory with fear and reward circuitry. Neurobiol Learn Mem 108:65-77.

Beier KT, Steinberg EE, DeLoach KE, Xie S, Miyamichi K, Schwarz L, Gao XJ, Kremer EJ, Malenka RC, Luo L (2015) Circuit Architecture of VTA Dopamine Neurons Revealed by Systematic Input-Output Mapping. Cell 162:622-634.

Berkes P, Orban G, Lengyel M, Fiser J (2011) Spontaneous cortical activity reveals hallmarks of an optimal internal model of the environment. Science 331:83-87.

Berridge KC, Robinson TE, Aldridge JW (2009) Dissecting components of reward: 'liking', 'wanting', and learning. Curr Opin Pharmacol 9:65-73.

Bromberg-Martin ES, Matsumoto M, Hikosaka O (2010) Dopamine in motivational control: rewarding, aversive, and alerting. Neuron 68:815-834.

Brown EN, Kass RE, Mitra PP (2004) Multiple neural spike train data analysis: state-of-the-art and future challenges. Nat Neurosci 7:456-461.

Buzsaki G (2010) Neural syntax: cell assemblies, synapsembles, and readers. Neuron 68:362-385.

Buzsaki G, Mizuseki K (2014) The log-dynamic brain: how skewed distributions affect network operations. Nat Rev Neurosci 15:264-278.

Caporale N, Dan Y (2008) Spike timing-dependent plasticity: a Hebbian learning rule. Annu Rev Neurosci 31:25-46.

Cohen MR, Maunsell JHR (2009) Attention improves performance primarily by reducing interneuronal correlations. Nat Neurosci 12:1594-1600.

Cox DR (1961) Tests of separate families of hypotheses. In: Proceedings of the fourth Berkeley symposium on mathematical statistics and probability, pp 105-123.

Cox DR (1962) Further results on tests of separate families of hypotheses. Journal of the Royal Statistical Society Series B (Methodological):406-424.

Cox DR (2013) A return to an old paper:'Tests of separate families of hypotheses'. Journal of the Royal Statistical Society: Series B (Statistical Methodology) 75:207-215.

Cui H, Andersen RA (2011) Different representations of potential and selected motor plans by distinct parietal areas. The Journal of neuroscience : the official journal of the Society for Neuroscience 31:18130-18136.

Cui Z, Feng R, Jacobs S, Duan Y, Wang H, Cao X, Tsien JZ (2013) Increased NR2A:NR2B ratio compresses long-term depression range and constrains long-term memory. Sci Rep 3:1036.

Dan Y, Felsen G, Touryan J (2009) Extracellular recording from cells in cat primary visual cortex. CRCNSorg.

deCharms RC, Zador A (2000) Neural representation and the cortical code. Annu Rev Neurosci 23:613-647.

DeWeese MR, Wehr M, Zador AM (2003) Binary spiking in auditory cortex. The Journal of neuroscience : the official journal of the Society for Neuroscience 23:7940-7949.

Ermentrout GB, Galan RF, Urban NN (2008) Reliability, synchrony and noise. Trends Neurosci 31:428-434.

Everitt BJ, Robbins TW (2005) Neural systems of reinforcement for drug addiction: from actions to habits to compulsion. Nat Neurosci 8:1481-1489.

Fadok JP, Dickerson TMK, Palmiter RD (2009) Dopamine is necessary for cue-dependent fear conditioning. The Journal of neuroscience : the official journal of the Society for Neuroscience 29:11089-11097.

Faisal AA, Selen LP, Wolpert DM (2008) Noise in the nervous system. Nat Rev Neurosci 9:292-303.

Felsen G, Touryan J, Han F, Dan Y (2005) Cortical sensitivity to visual features in natural scenes. PLoS Biol 3:e342.

Gerstner W, Naud R (2009) Neuroscience. How good are neuron models? Science 326:379-380.

Gerstner W, Kempter R, van Hemmen JL, Wagner H (1996) A neuronal learning rule for sub-millisecond temporal coding. Nature 383:76-81.

Gilson M, Masquelier T, Hugues E (2011) STDP allows fast rate-modulated coding with Poisson-like spike trains. PLoS Comput Biol 7:e1002231.

Grace AA (2000) The tonic/phasic model of dopamine system regulation and its implications for understanding alcohol and psychostimulant craving. Addiction 95 Suppl 2:S119-128.

Gupta AS, van der Meer MA, Touretzky DS, Redish AD (2010) Hippocampal replay is not a simple function of experience. Neuron 65:695-705.

Hamel-Pâquet C, Sergio LE, Kalaska JF (2006) Parietal area 5 activity does not reflect the differential time-course of motor output kinetics during arm-reaching and isometric-force tasks. J Neurophysiol 95:3353-3370.

Heil P, Neubauer H, Irvine DRF, Brown M (2007) Spontaneous activity of auditory-nerve fibers: insights into stochastic processes at ribbon synapses. The Journal of neuroscience : the official journal of the Society for Neuroscience 27:8457-8474.

Jacobs S, Cui Z, Feng R, Wang H, Wang D, Tsien JZ (2014) Molecular and genetic determinants of the NMDA receptor for superior learning and memory functions. PloS one 9:e111865.

Kang J, Wu J, Smerieri A, Feng J (2010) Weber's law implies neural discharge more regular than a Poisson process. The European journal of neuroscience 31:1006-1018.

Kara P, Reinagel P, Reid RC (2000) Low response variability in simultaneously recorded retinal, thalamic, and cortical neurons. Neuron 27:635-646.

Kuang H, Lin L, Tsien JZ (2010) Temporal dynamics of distinct CA1 cell populations during unconscious state induced by ketamine. PLoS One 5:e15209.

Lammel S, Ion DI, Roeper J, Malenka RC (2011) Projection-specific modulation of dopamine neuron synapses by aversive and rewarding stimuli. Neuron 70:855-862.

Li M, Zhao F, Lee J, Wang D, Kuang H, Tsien JZ (2015) Computational Classification Approach to Profile Neuron Subtypes from Brain Activity Mapping Data. Sci Rep 5:12474.

Li Y, Cui H (2013) Dorsal parietal area 5 encodes immediate reach in sequential arm movements. The Journal of neuroscience : the official journal of the Society for Neuroscience 33:14455-14465.

Lin L, Chen G, Xie K, Zaia KA, Zhang S, Tsien JZ (2006) Large-scale neural ensemble recording in the brains of freely behaving mice. J Neurosci Methods 155:28-38.

Lindner B (2006) Superposition of many independent spike trains is generally not a Poisson process. Physical Review E 73:022901.

Lisman J, Spruston N (2005) Postsynaptic depolarization requirements for LTP and LTD: a critique of spike timing-dependent plasticity. Nat Neurosci 8:839-841.

Ma WJ, Beck JM, Latham PE, Pouget A (2006) Bayesian inference with probabilistic population codes. Nature neuroscience 9:1432-1438.

Maimon G, Assad JA (2009) Beyond Poisson: increased spike-time regularity across primate parietal cortex. Neuron 62:426-440.

Mainen ZF, Sejnowski TJ (1995) Reliability of spike timing in neocortical neurons. Science 268:1503-1506.

Markram H, Lubke J, Frotscher M, Sakmann B (1997) Regulation of synaptic efficacy by coincidence of postsynaptic APs and EPSPs. Science 275:213-215.

Masquelier T (2013) Neural variability, or lack thereof. Front Comput Neurosci 7:7.

Mazurek ME, Shadlen MN (2002) Limits to the temporal fidelity of cortical spike rate signals. Nature neuroscience 5:463-471.

Mitchell JF, Sundberg KA, Reynolds JH (2007) Differential attention-dependent response modulation across cell classes in macaque visual area V4. Neuron 55:131-141.

Mitchell JF, Sundberg KA, Reynolds JH (2009) Spatial attention decorrelates intrinsic activity fluctuations in macaque area V4. Neuron 63:879-888.

Mizuseki K, Buzsaki G (2013) Preconfigured, skewed distribution of firing rates in the hippocampus and entorhinal cortex. Cell Rep 4:1010-1021.

Moezzi B, Iannella N, McDonnell MD (2016) Ion channel noise can explain firing correlation in auditory nerves. J Comput Neurosci 41:193-206.

Monyer H, Sprengel R, Schoepfer R, Herb A, Higuchi M, Lomeli H, Burnashev N, Sakmann B, Seeburg PH (1992) Heteromeric NMDA receptors: molecular and functional distinction of subtypes. Science 256:1217-1221.

Niell CM, Stryker MP (2010) Modulation of visual responses by behavioral state in mouse visual cortex. Neuron 65:472-479.

Paxinos G, Franklin KB (2004) The mouse brain in stereotaxic coordinates: Gulf Professional Publishing.

Pezze MA, Feldon J (2004) Mesolimbic dopaminergic pathways in fear conditioning. Prog Neurobiol 74:301-320.

Pipa G, Grun S, van Vreeswijk C (2013) Impact of spike train autostructure on probability distribution of joint spike events. Neural Comput 25:1123-1163.

Preston RJ, Bishop GA, Kitai ST (1980) Medium spiny neuron projection from the rat striatum: an intracellular horseradish peroxidase study. Brain Res 183:253-263.

Schmitzer-Torbert N, Jackson J, Henze D, Harris K, Redish AD (2005) Quantitative measures of cluster quality for use in extracellular recordings. Neuroscience 131:1-11.

Schultz W (2013) Updating dopamine reward signals. Current opinion in neurobiology 23:229-238.

Shadlen MN, Newsome WT (1994) Noise, neural codes and cortical organization. Curr Opin Neurobiol 4:569-579.

Shadlen MN, Newsome WT (1998) The variable discharge of cortical neurons: implications for connectivity, computation, and information coding. The Journal of neuroscience : the official journal of the Society for Neuroscience 18:3870-3896.

Sheng M, Cummings J, Roldan LA, Jan YN, Jan LY (1994) Changing subunit composition of heteromeric NMDA receptors during development of rat cortex. Nature 368:144-147.

Sjostrom PJ, Turrigiano GG, Nelson SB (2001) Rate, timing, and cooperativity jointly determine cortical synaptic plasticity. Neuron 32:1149-1164.

Song S, Miller KD, Abbott LF (2000) Competitive Hebbian learning through spike-timing-dependent synaptic plasticity. Nat Neurosci 3:919-926.

Surmeier DJ, Ding J, Day M, Wang Z, Shen W (2007) D1 and D2 dopamine-receptor modulation of striatal glutamatergic signaling in striatal medium spiny neurons. Trends Neurosci 30:228-235.

Swanson LW (1982) The projections of the ventral tegmental area and adjacent regions: a combined fluorescent retrograde tracer and immunofluorescence study in the rat. Brain Res Bull 9:321-353.

Tang YP, Shimizu E, Dube GR, Rampon C, Kerchner GA, Zhuo M, Liu G, Tsien JZ (1999) Genetic enhancement of learning and memory in mice. Nature 401:63-69.

Toups JV, Fellous J-M, Thomas PJ, Sejnowski TJ, Tiesinga PH (2012) Multiple spike time patterns occur at bifurcation points of membrane potential dynamics. PLoS Comput Biol 8:e1002615.

Touryan J, Lau B, Dan Y (2002) Isolation of relevant visual features from random stimuli for cortical complex cells. The Journal of neuroscience : the official journal of the Society for Neuroscience 22:10811-10818.

Touryan J, Felsen G, Dan Y (2005) Spatial structure of complex cell receptive fields measured with natural images. Neuron 45:781-791.

Wang DV, Tsien JZ (2011) Convergent processing of both positive and negative motivational signals by the VTA dopamine neuronal populations. PloS one 6:e17047.

Wise RA (2004) Dopamine, learning and motivation. Nat Rev Neurosci 5:483-494.

Xie K, Fox GE, Liu J, Tsien JZ (2016a) 512-Channel and 13-Region Simultaneous Recordings Coupled with Optogenetic Manipulation in Freely Behaving Mice. Front Syst Neurosci 10:48.

Xie K, Fox GE, Liu J, Lyu C, Lee JC, Kuang H, Jacobs S, Li M, Liu T, Song S, Tsien JZ (2016b) Brain Computation Is Organized via Power-of-Two-Based Permutation Logic. Front Syst Neurosci 10:95.

Figure Legends

Figure 1. Statistical properties of neural spike patterns

(**A**) Spikes are highly variable. The upper subpanel illustrates the spike-activity patterns of 20 neurons within a 10-sec time period recorded from the VTA region of a mouse during the awake state. The lower subpanel shows the ISI distribution of a sample neuron.

(**B**) Illustrations of a positive- and negative-skewed distribution. The red and blue curves illustrate a positive-skewed distribution and a negative-skewed distribution, respectively. Gray dashed lines denoted symmetric distributions. The positive/negative-skewed properties are examined by using skewness (γ) and nonparametric-skew (S).

(**C**) Illustrations of a gamma distribution model and a log-normal distribution model. Shown is fitted gamma distribution and log-normal distribution of the ISI distribution in the lower subpanel of (**A**). The goodness-of-fit analysis is conducted to compare the gamma distribution model to the log-normal distribution model for characterizing neuronal spike patterns.

Figure 2. Putative principal cells in mice's cortical and subcortical regions discharge positive-skewed, heavy-tailed spike patterns.

(**A**) ACC, (**B**) RSC, (**C**) CA1 and (**D**) BLA. The left subpanels of (**A**-**D**) show the histograms of skewness γ in the corresponding regions, where the gray vertical lines (γ=0) denote the symmetric distributions, positive-skewed distributions have $\gamma > 0$, and negative-skewed distributions have $\gamma < 0$. The middle subpanels of (**A**-**D**) show the histograms of nonparametric-skew S in the corresponding regions, the symmetric distributions have $S = 0$, $S > 0$ for positive-skewed distributions and $S < 0$ for negative-skewed distributions. The right subpanels of (**A**-**D**) show their relationships with the neurons' firing rates, where the colors of each dot represent the firing rates of corresponding neurons.

Figure 3. Spike patterns of principal cells followed gamma distribution across different mice cortical and subcortical regions under the quiet-awake state.

(**A**) ACC, (**B**) RSC, (**C**) CA1 and (**D**) BLA. The left subpanels of (**A**-**D**) show the neuronal spike patterns of sample neurons recorded from corresponding brain regions, and their fitted gamma distributions (red curves) and log-normal distributions (blue curves). The right subpanels of (**A**-**D**) are the distributions of D (the natural logarithm of RML) vs. mean firing rates of principal cells under the quiet-awake state. The lines illustrate the linear relations (linear regression) between D and mean firing rates of principal cells in corresponding regions.

Figure 4. Spike patterns of principal cells followed gamma distribution across different mice cortical and subcortical regions during the animals' sleep.

The distributions of D (the natural logarithm of RML) vs. mean firing rates of principal cells recorded from different cortical and subcortical regions during the animals' sleep. The lines illustrate the linear relations (linear regression) between D and mean firing rates of principal cells in corresponding regions.

Figure 5. Preserved shape parameter *k* across brain states.

Distributions of shape parameter k of principal cells during awake and sleep states are shown in the left subpanels of (**A-D**), while distributions of scale parameter θ in these two states are shown in the right subpanels of (**A-D**). Red lines denote the linear regressions of corresponding parameters, red numbers at the upper-left corner of each subpanel denote the correlation coefficients.

Figure 6. Neuronal spike-activity patterns of medium spiny projection neurons followed gamma distribution.

(**A**) Neuronal spike pattern of sample medium spiny projection neurons recorded from the dorsal striatum of mice, and its fitted gamma distribution (red curve) and log-normal distribution (blue curve).

(**B**) Medium spiny projection neurons discharge positive-skewed, heavy-tailed spike patterns. The upper subpanel: the histogram of γ. The middle subpanel: the histogram of S. The lower subpanel: the distribution of γ and S, where the colors of each dot represent neurons' firing rates.

(**C**) The distribution of D vs. mean firing rates of medium spiny projection neurons. The line in the plot denotes the linear relation between D and mean firing rates of corresponding neurons.

Figure 7. Neuronal spike-activity patterns of VTA DA neurons followed gamma distribution.

(**A**) Fitted gamma distribution and log-normal distribution of a sample DA neuron recorded from mice VTA region.

(**B**) VTA DA neurons discharge positive-skewed, heavy-tailed spike patterns. The upper subpanel: the histogram of γ. The middle-subpanel: the histogram of S. The lower subpanel: the distribution of γ and S, where the colors of each dot represent neurons' firing rates.

(**C**) The distribution of D vs. mean firing rates of VTA DA neurons. The line in the plot denotes the linear relation between D and mean firing rates of corresponding neurons.

Figure 8. Neuronal spike-activity patterns of principal cells in hamster PrL region followed gamma distribution.

(**A**) Fitted gamma distribution and log-normal distribution of a sample principal cell recorded from a hamster PrL region.

(**B**) Principal cells in a hamster PrL region discharge positive-skewed, heavy-tailed spike patterns. The upper subpanel: the histogram of γ. The middle subpanel: the histogram of S. The lower subpanel: the distribution of γ and S, where the colors of each dot represent neurons' firing rates.

(**C**) The distribution of D vs. mean firing rates of principal cells in the hamster PrL region. The line in the plot denotes the linear relation between D and mean firing rates of corresponding neurons.

Figure 9. Neuronal spike-activity patterns of neurons in area 5d of a monkey followed gamma distribution.

(**A**) Fitted gamma distribution and log-normal distribution of a sample neuron recorded from area 5d of a monkey.

(**B**) Neurons in area 5d discharge positive-skewed, heavy-tailed spike patterns. The upper subpanel: the histogram of γ. The middle-subpanel: the histogram of S. The lower subpanel: the distribution of γ and S, where the colors of each dot represent neurons' firing rates.

(**C**) The distribution of D vs. mean firing rates of neurons in area 5d. The line in the plot denotes the linear relation between D and mean firing rates of corresponding neurons.

Figure 10. Neuronal spike-activity patterns of neurons in the primary visual cortex of cats followed gamma distribution.

(**A** and **B**) Fitted gamma distributions and log-normal distributions of sample neurons recorded from the primary visual cortex of cats under 1-D white noise (**A**) and 2-D stimuli (**B**).

(**C** and **D**) Neurons in the primary visual cortex of cats discharge positive-skewed, heavy-tailed spike patterns under 1-D white noise (**C**) and 2-D stimuli (**D**). The upper subpanels: the histograms of γ. The middle subpanels: the histograms of S. The lower subpanels: the distributions of γ and S, where the colors of each dot represent neurons' firing rates.

(**E** and **F**) The distributions of D vs. mean firing rates of neurons in the primary visual cortex of cats under 1-D white noise (**E**) and 2-D stimuli (**F**). The lines in the plots denote the linear relations between D and mean firing rates of corresponding neurons.

Figure 11. Neuronal spike-activity patterns' regularities across distinct brain regions of different species.

The distributions of shape parameter k in 13 brain regions recorded from four different mammalian species. Each dot represents a neuron. The gray horizontal line denotes the Poisson process ($k=1$), regular spiking ($k>1$) and irregular spiking ($k<1$) were shown as a red-arrow line and blue-arrow line, respectively. The error bars denoted mean ± SEM.

A

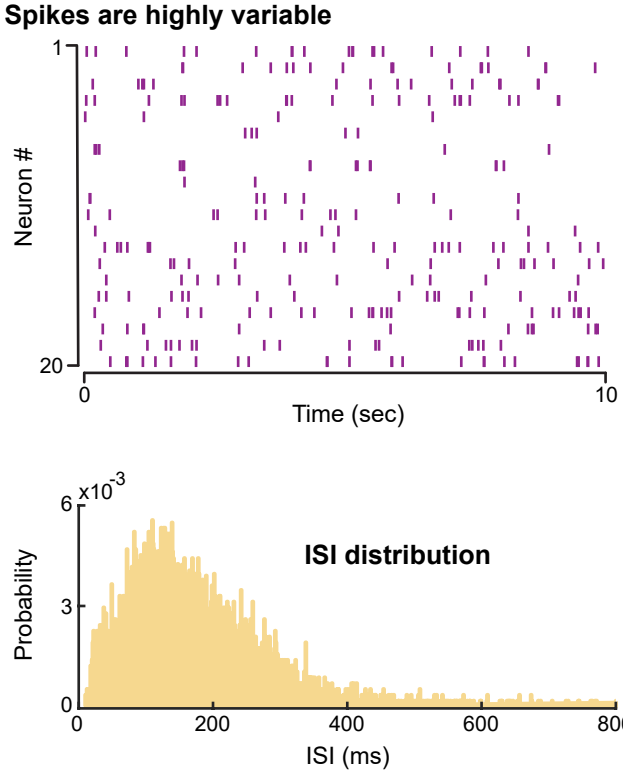
Spikes are highly variable
Neuron #
1
20
0
10
Time (sec)
x10-3
6
3
0
Probability
ISI distribution
0
200
400
600
800
ISI (ms)

B

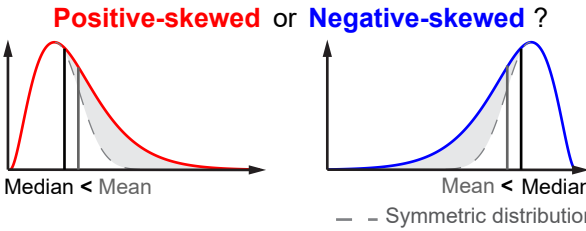
Positive-skewed or Negative-skewed ?
Median < Mean
Mean < Median
Symmetric distribution

C

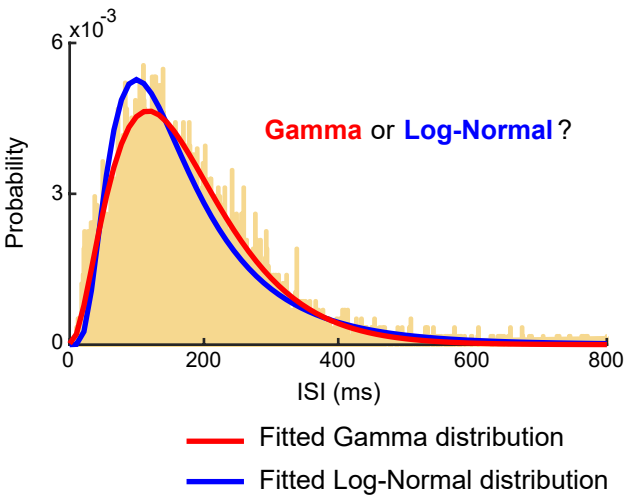
x10-3
6
3
0
Probability
Gamma or Log-Normal ?
0
200
400
600
800
ISI (ms)
Fitted Gamma distribution
Fitted Log-Normal distribution

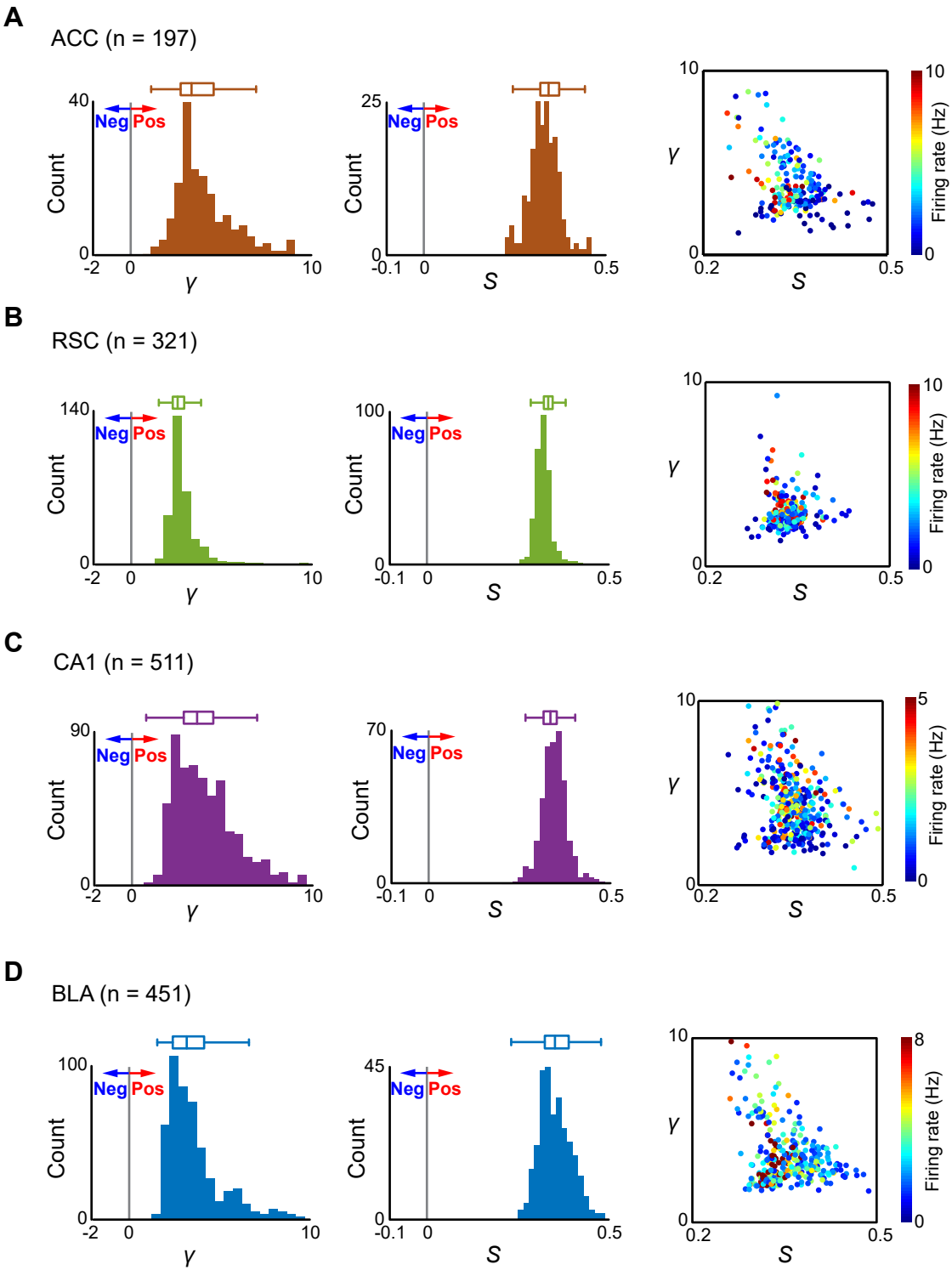
A
ACC (n = 197)
Neg
Pos
Count
γ
S
Firing rate (Hz)
B
RSC (n = 321)
C
CA1 (n = 511)
D
BLA (n = 451)

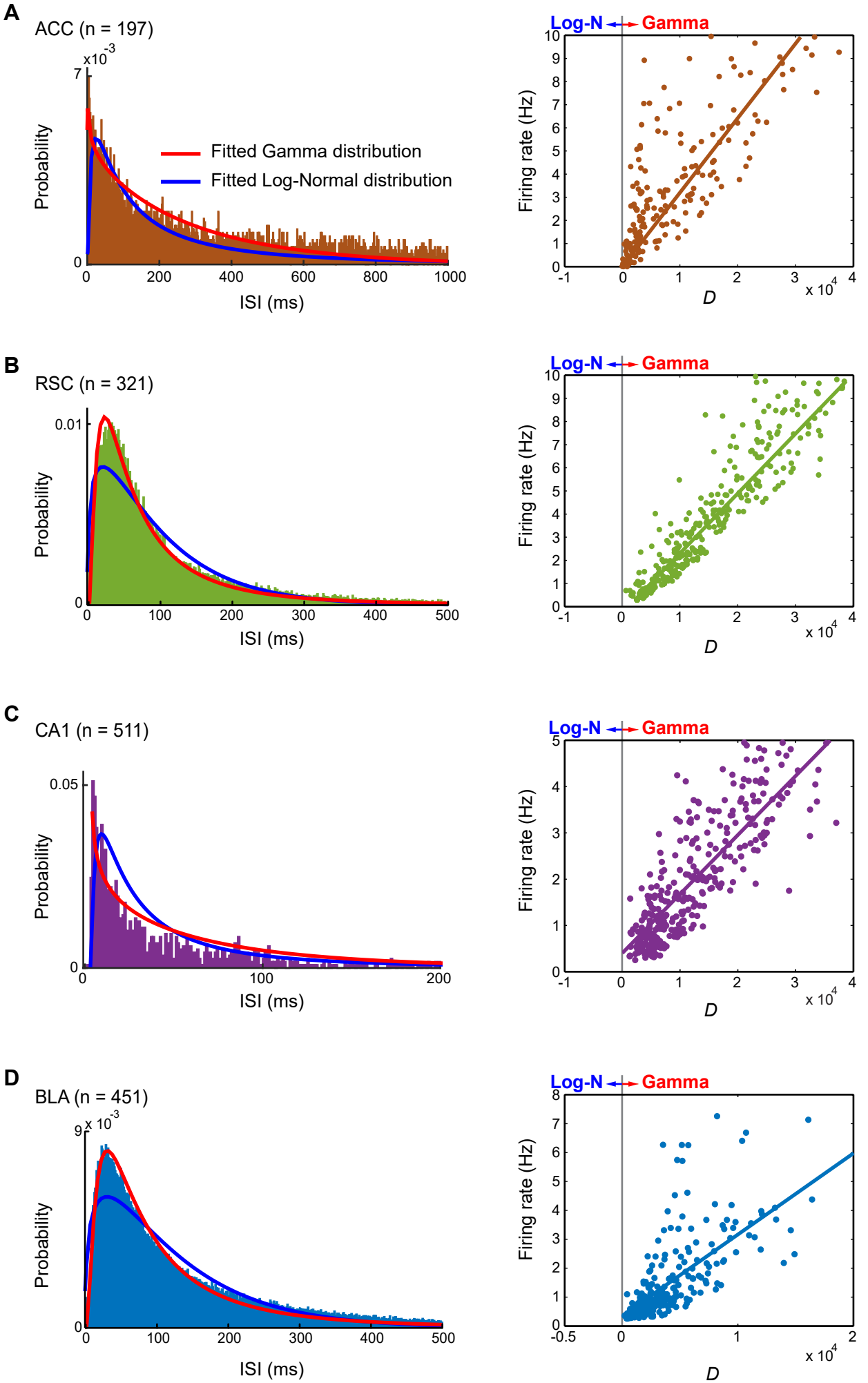

Figure 4

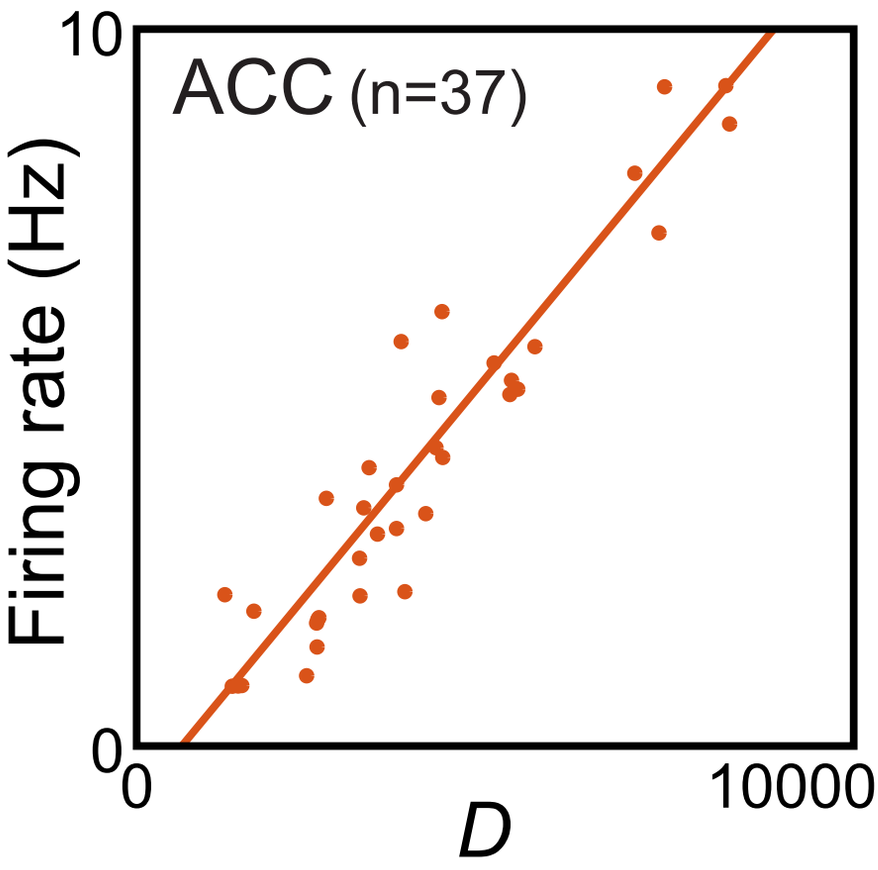
ACC (n=37)
Firing rate (Hz)
10
0
0
10000
D

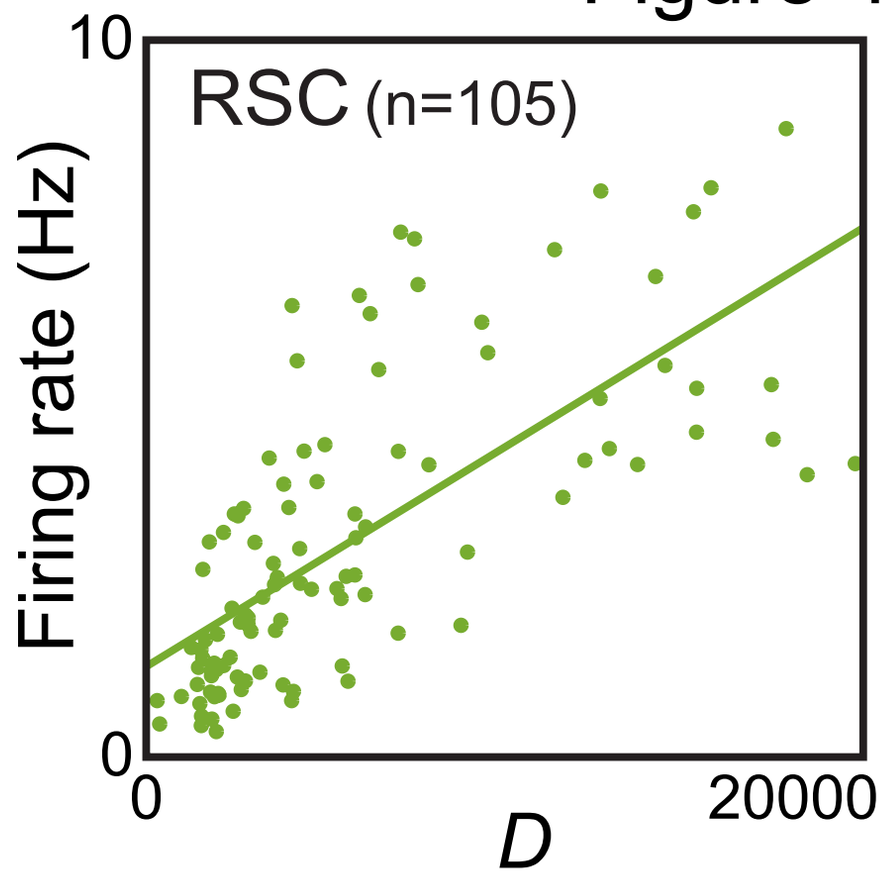
RSC (n=105)
Firing rate (Hz)
10
0
0
20000
D

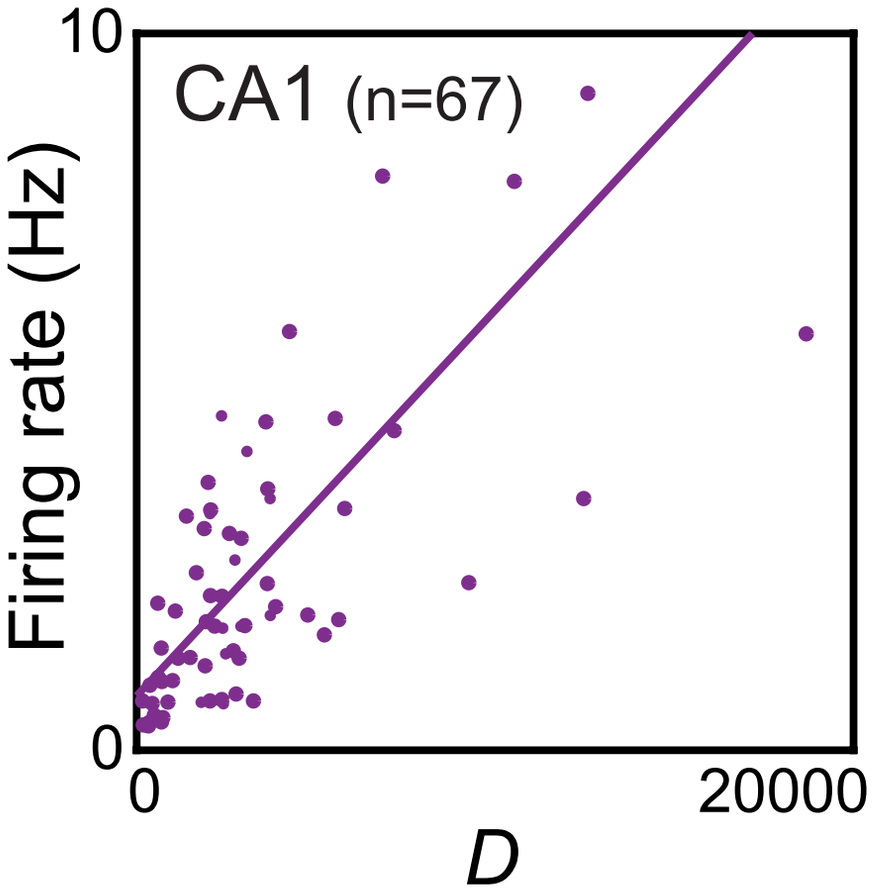
CA1 (n=67)
Firing rate (Hz)
10
0
0
20000
D

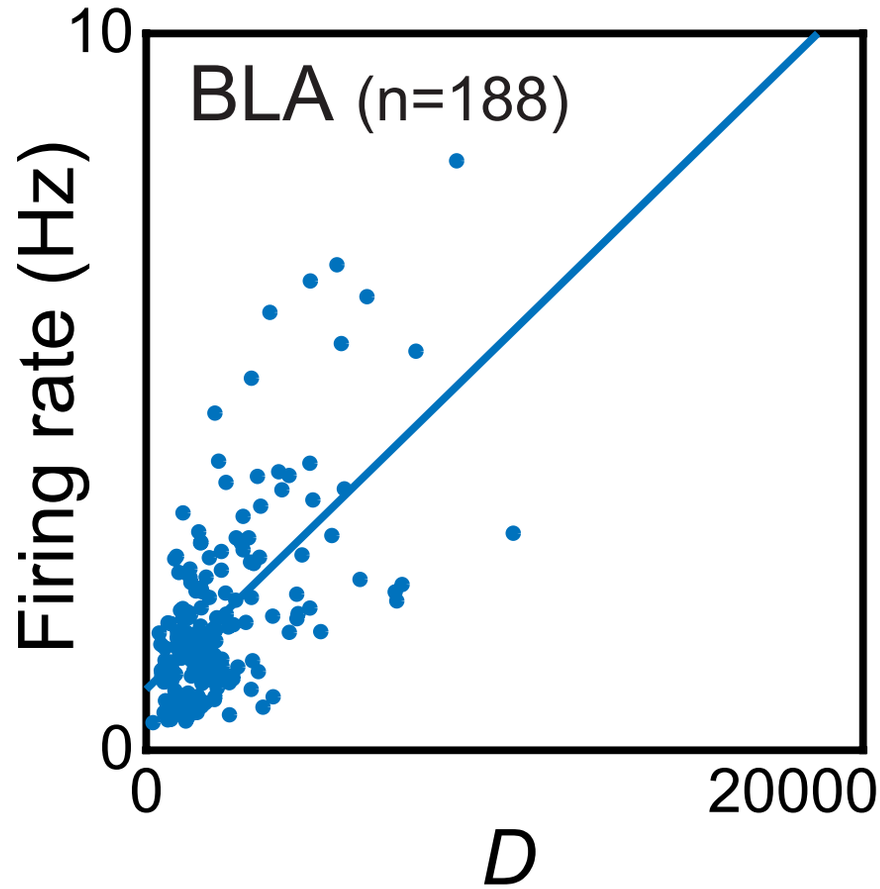
BLA (n=188)
Firing rate (Hz)
10
0
0
20000
D

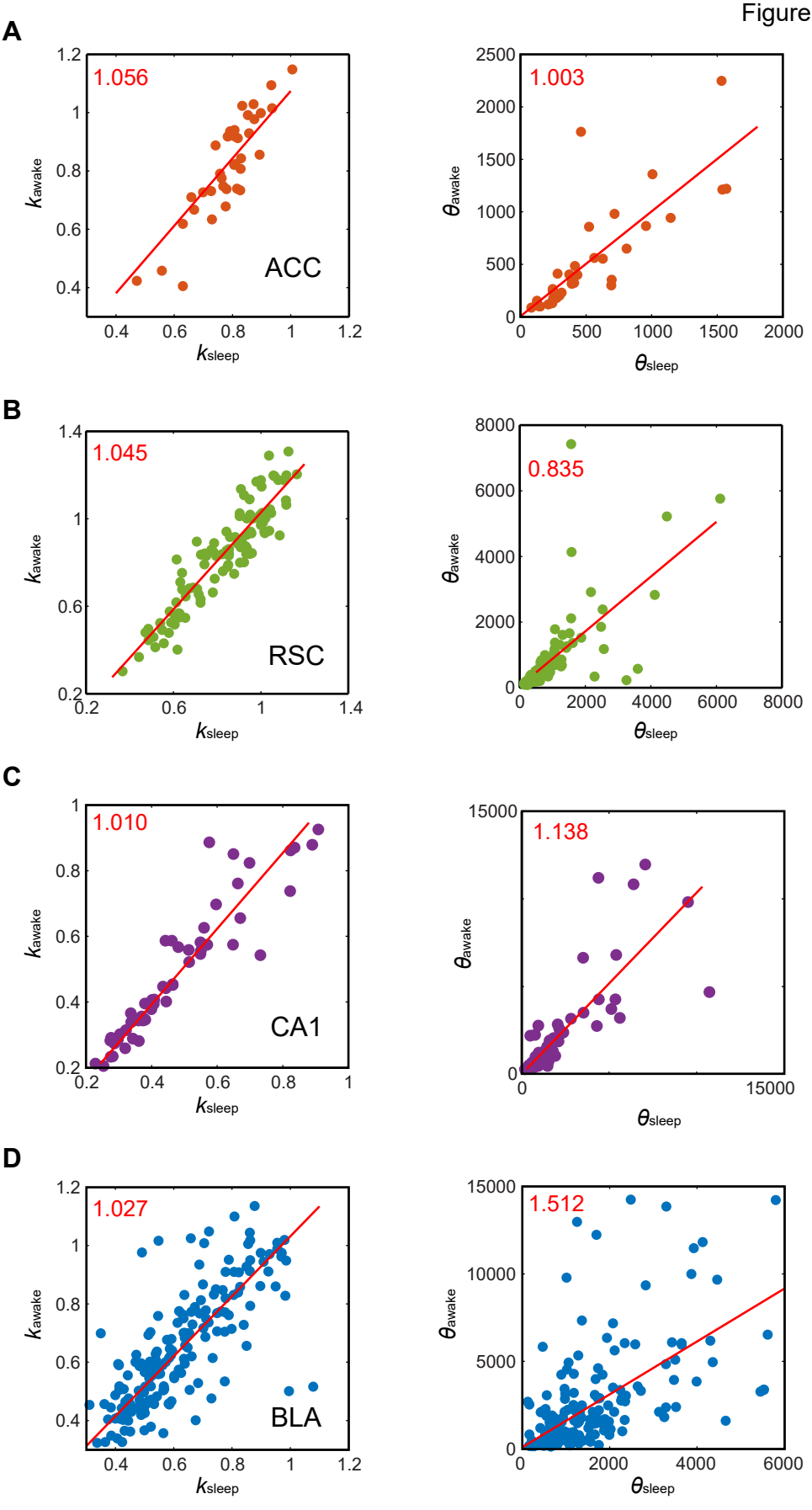
A
1.056
ACC
k_{awake}
k_{sleep}
1.003
θ_{awake}
θ_{sleep}
B
1.045
RSC
k_{awake}
k_{sleep}
0.835
θ_{awake}
θ_{sleep}
C
1.010
CA1
k_{awake}
k_{sleep}
1.138
θ_{awake}
θ_{sleep}
D
1.027
BLA
k_{awake}
k_{sleep}
1.512
θ_{awake}
θ_{sleep}

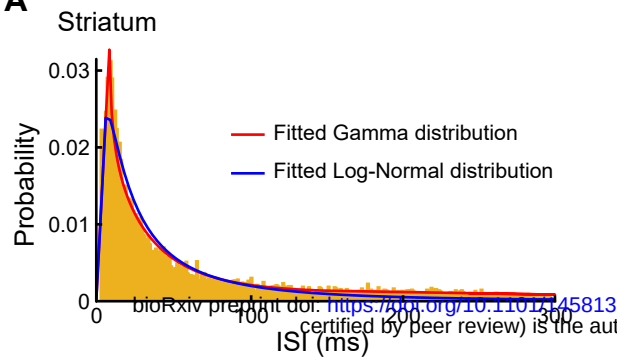

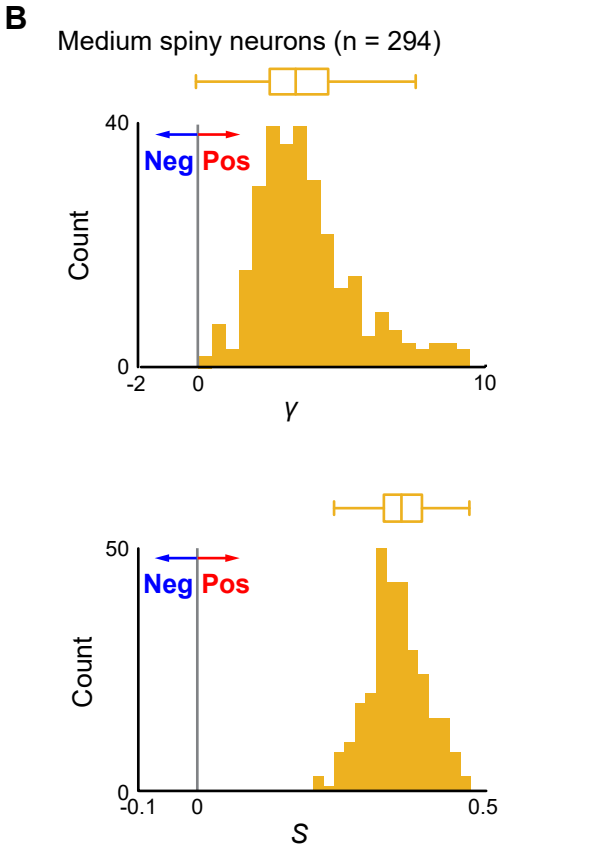

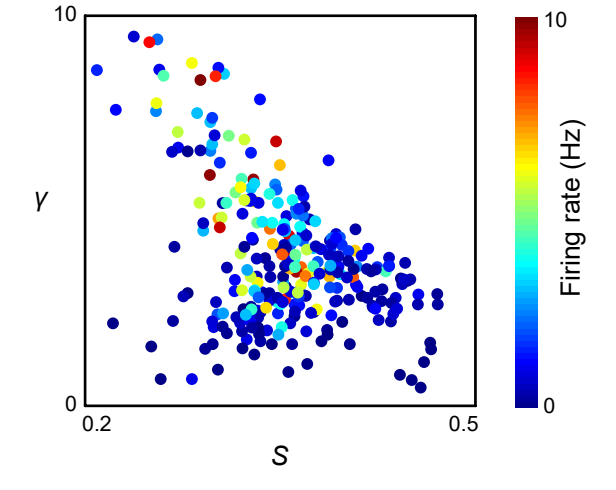

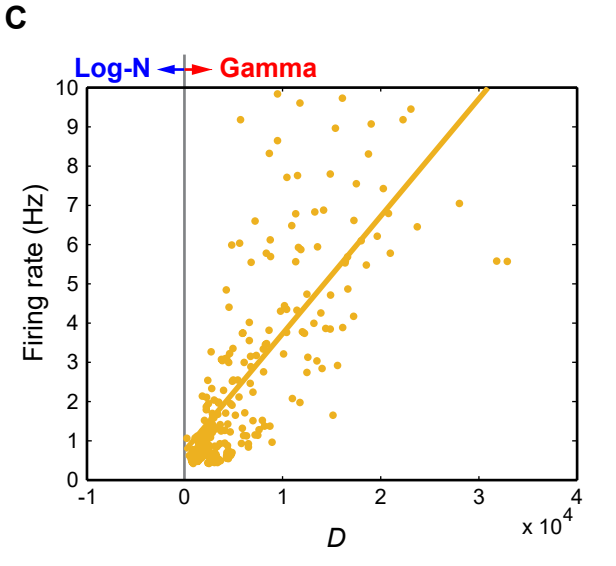

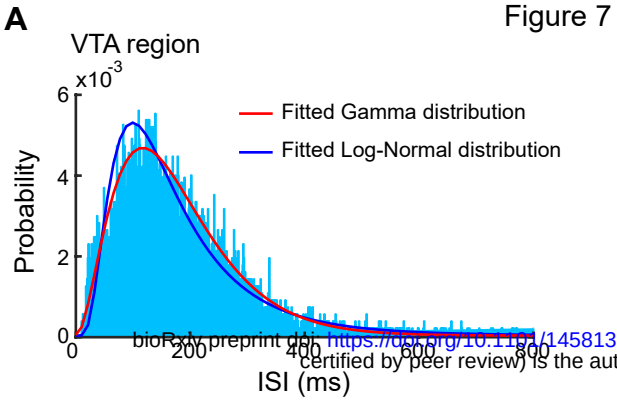

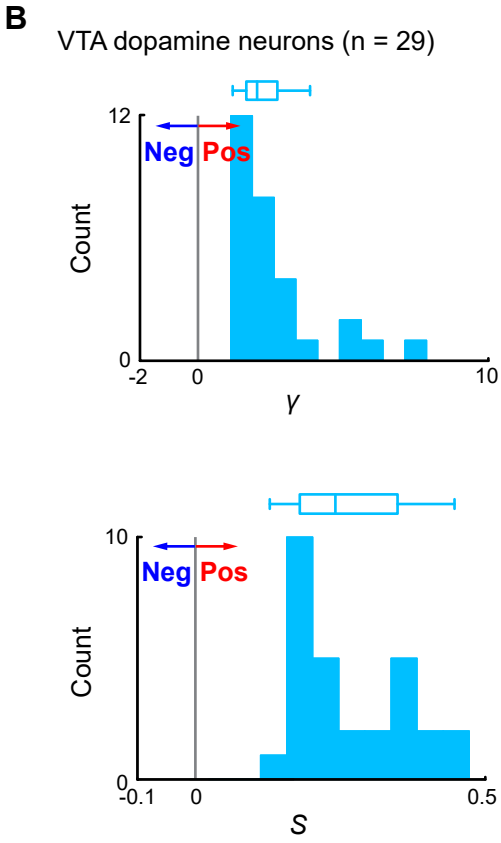

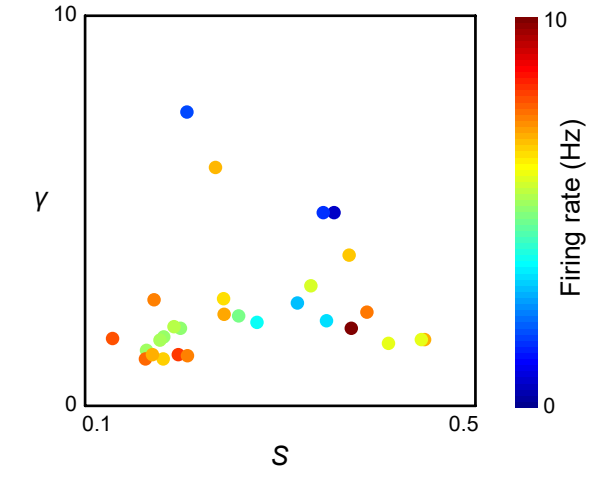

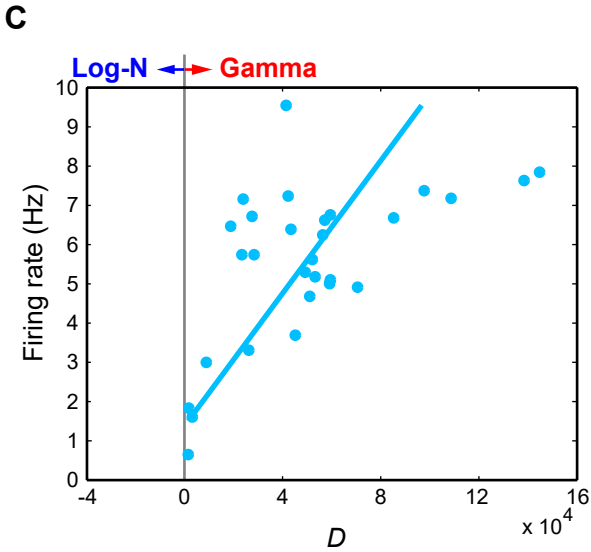

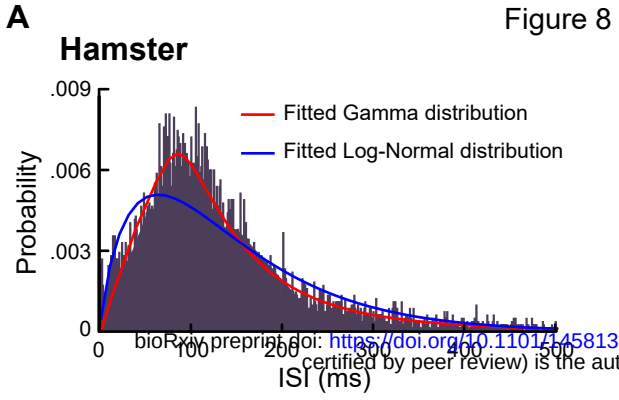

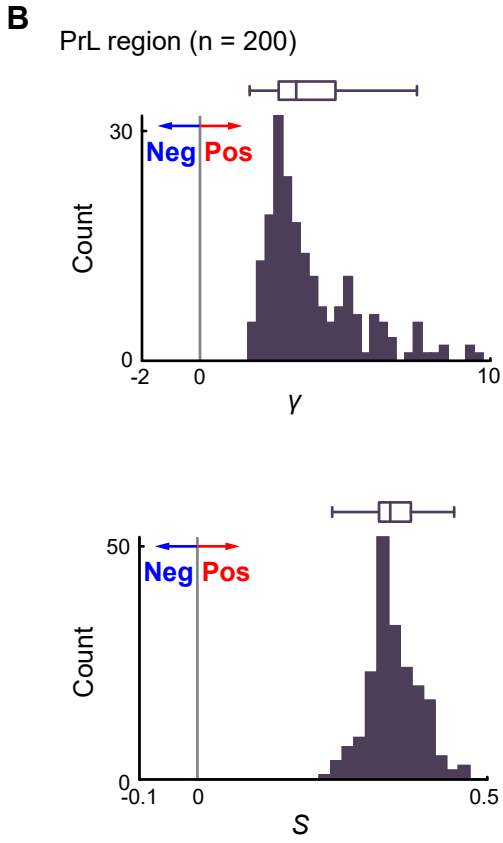

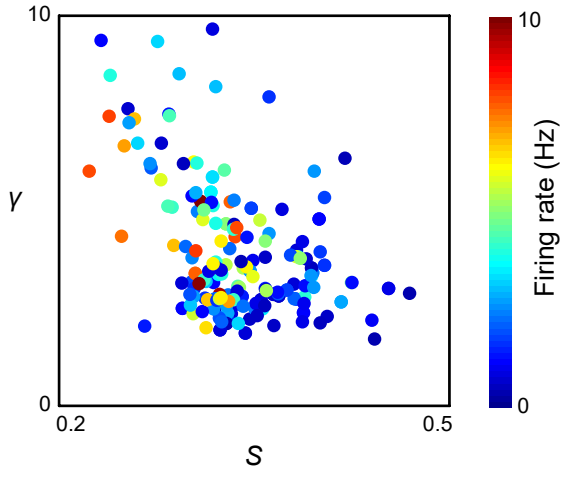

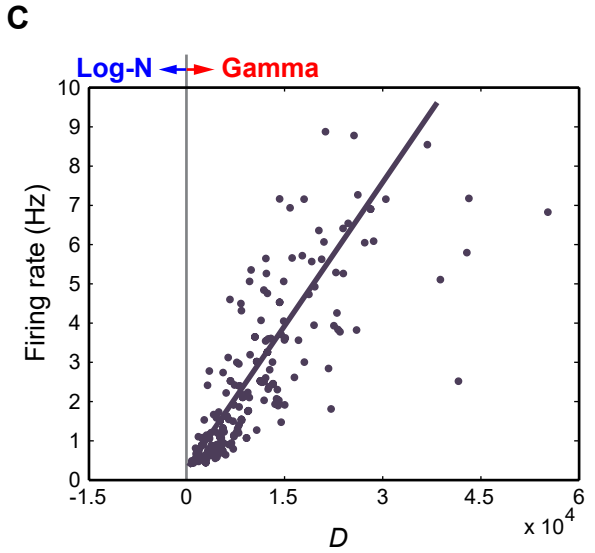

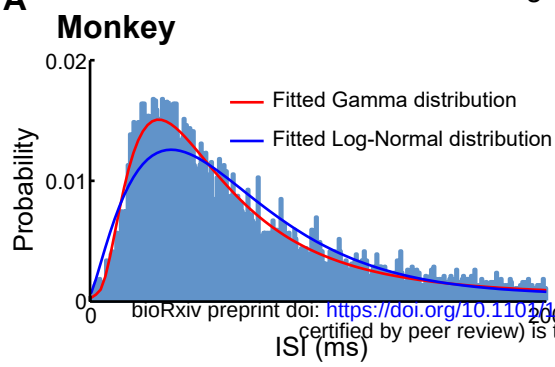

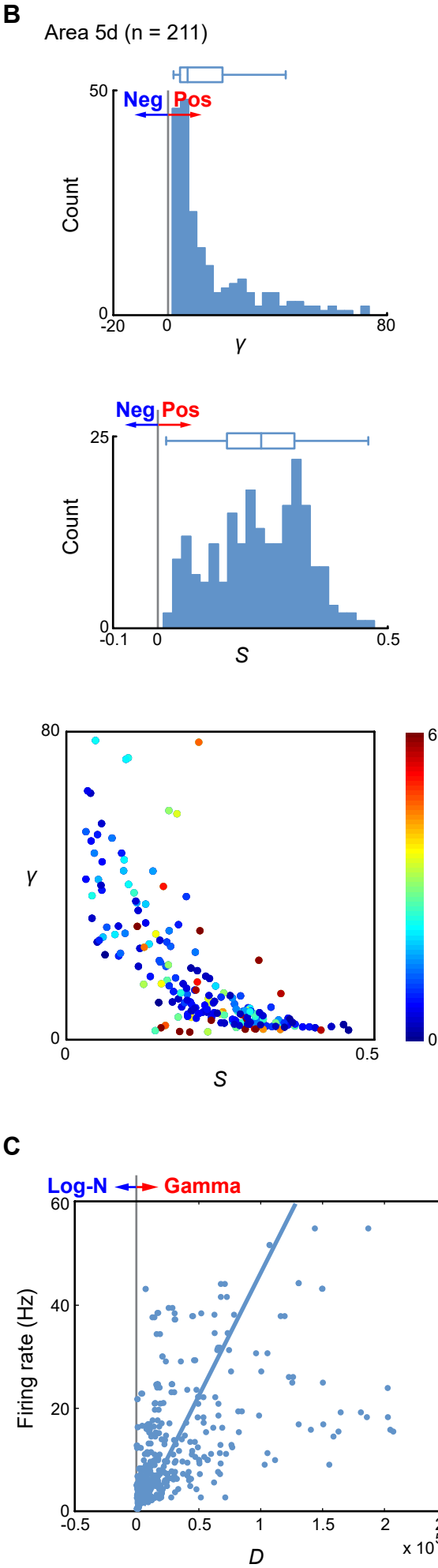

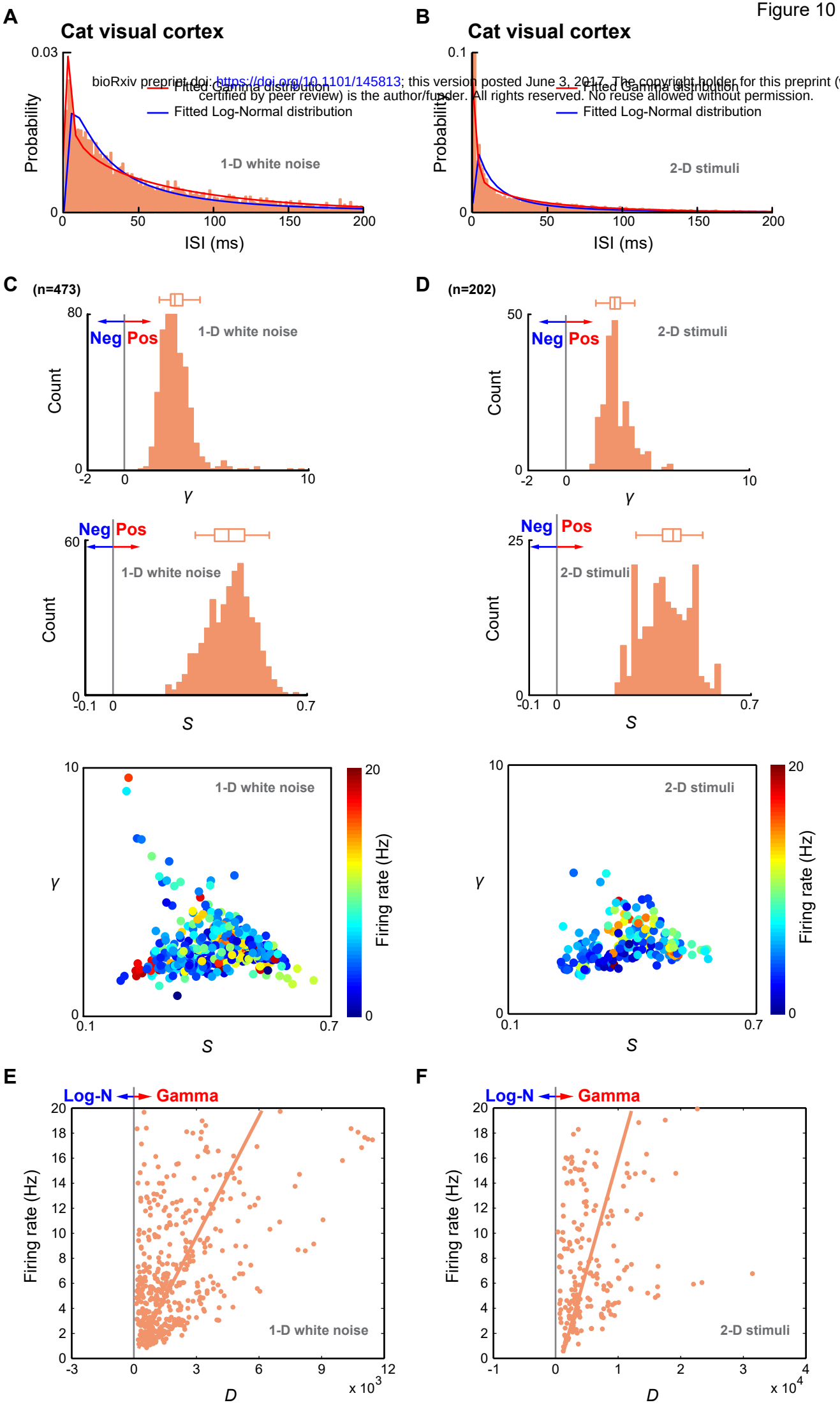

Figure 11

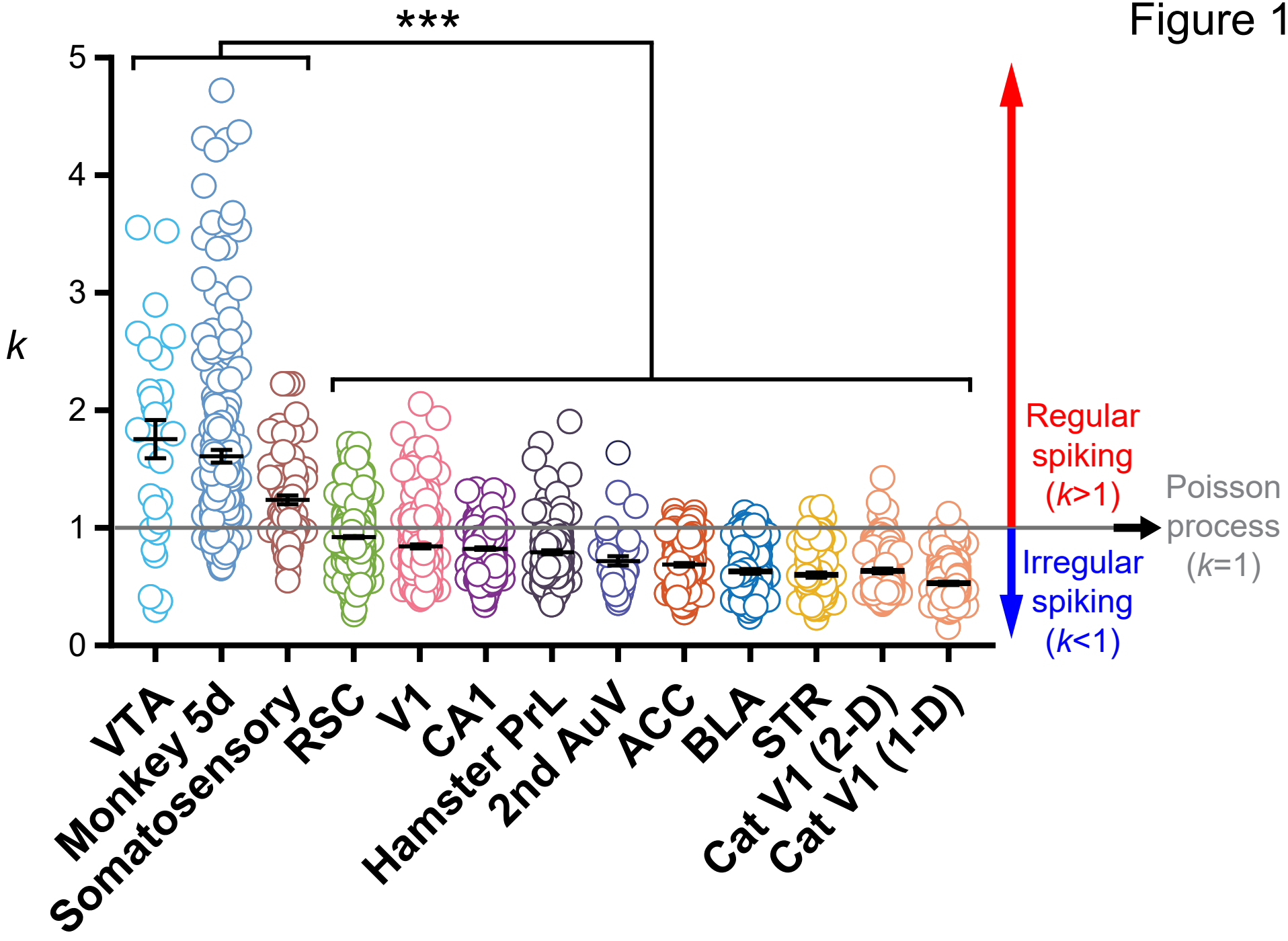
***
5
4
3
2
1
0
k
Regular spiking (k>1)
Irregular spiking (k<1)
Poisson process (k=1)
VTA
Monkey 5d Somatosensory
RSC
V1
CA1
Hamster PrL
2nd AuV
ACC
BLA
STR
Cat V1 (2-D)
Cat V1 (1-D)